BIOCHEMISTRY
including biophysical chemistry & molecular biology

Article

pubs.acs.org/biochemistry

1,2,3-Triazole−Heme Interactions in Cytochrome P450: Functionally Competent Triazole−Water−Heme Complexes

Kip P. Conner,[†] Preethi Vennam,[‡] Caleb M. Woods,[†] Matthew D. Krzyaniak,[‡] Michael K. Bowman,[‡] and William M. Atkins*[,†]

[†]Department of Medicinal Chemistry, Box 357610, University of Washington, Seattle, Washington 98195-7610, United States
[‡]Department of Chemistry, University of Alabama, Tuscaloosa, Alabama 35487-0336, United States

Supporting Information

ABSTRACT: In comparison to imidazole (IMZ) and 1,2,4-triazole (1,2,4-TRZ), the isosteric 1,2,3-triazole (1,2,3-TRZ) is unrepresented among cytochrome P450 (CYP) inhibitors. This is surprising because 1,2,3-TRZs are easily obtained via "click" chemistry. To understand this underrepresentation of 1,2,3-TRZs among CYP inhibitors, thermodynamic and density functional theory computational studies were performed with unsubstituted IMZ, 1,2,4-TRZ, and 1,2,3-TRZ. The results indicate that the lower affinity of 1,2,3-TRZ for the heme iron includes a large unfavorable entropy term likely originating in solvent−1,2,3-TRZ interactions; the difference is not solely due to differences in the enthalpy of heme−ligand interactions. In addition, the 1,2,3-TRZ fragment was incorporated into a well-established CYP3A4 substrate and mechanism-based inactivator, 17-α-ethynylestradiol (17EE), via click chemistry. This derivative, 17-click, yielded optical spectra consistent with low-spin ferric heme iron (type II) in contrast to 17EE, which yields a high-spin complex (type I). Furthermore, the rate of CYP3A4-mediated metabolism of 17-click was comparable to that of 17EE, with a different regioselectivity. Surprisingly, continuous-wave electron paramagnetic resonance (EPR) and HYSCORE EPR spectroscopy indicate that 17-click does not displace water from the sixth axial ligand position of CYP3A4 as expected for a type II ligand. We propose a binding model in which 17-click pendant 1,2,3-TRZ hydrogen bonds with the sixth axial water ligand. The results demonstrate the potential for 1,2,3-TRZ to form metabolically labile water-bridged low-spin heme complexes, consistent with recent evidence that nitrogenous type II ligands of CYPs can be efficiently metabolized. The specific case of [CYP3A4·17-click] highlights the risk of interpreting CYP−ligand complex structure on the basis of optical spectra.

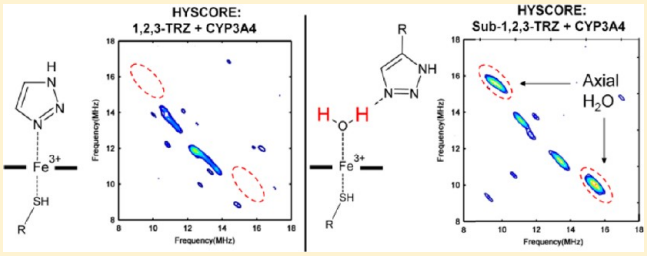

Cytochrome P450 (CYP)−heme interactions with nitrogenous drugs contribute to the pharmacology of a wide range of therapeutic agents. Collectively, CYPs represent both therapeutic targets and critical determinants of drug metabolism and drug−drug interactions. For example, drugs targeted to aromatase (CYP19) for use in breast cancer,[1] to lanosterol demethylase (CYP51A1) for antifungal therapy,[2] or to other CYPs expressed in infectious pathogens[3] exploit heme−imidazole or heme−triazole interactions. Similar heme−nitrogen interactions are often considered to be a component of inhibition of the drug-metabolizing CYPs, and such inhibitors can alter the clearance of other drugs.[4] However, recent studies[5−7] demonstrate that the heme−nitrogen interactions are not exclusively "inhibitory", and our fundamental understanding of the interaction between nitrogenous drugs and the heme group of CYPs is incomplete.

Surprisingly, all marketed azole drugs designed to exploit heme−nitrogen interactions with CYPs are either imidazole (IMZ)-, 1,2,4-triazole (1,2,4-TRZ)-, or thiazole-based despite the extraordinary synthetic advantages of 1,2,3-triazoles (1,2,3-TRZs).[8,9] Although several studies have suggested[10,11] that, despite their lower basicity, the 1,2,3-TRZs can ligate to the heme iron of CYPs, they are conspicuously absent among marketed CYP inhibitors. In the absence of significant confounding problems, 1,2,3-TRZs, in principle, could be a powerful element of fragment-based anti-CYP drug discovery. To determine whether 1,2,3-TRZs have unique properties among isosteric nitrogen heterocycles, we have compared the spectroscopic and thermodynamic behavior of binding of 1,2,3-TRZ to CYPs with that of IMZ and 1,2,4-TRZ. We also provide a spectral and functional characterization of a well-established CYP3A4 inhibitor after installation of a 1,2,3-TRZ on its molecular framework. The results indicate that interactions of heme with 1,2,3-TRZs include unusual structural features that could explain the limitations of this fragment in CYP inhibitor discovery but could be exploited to "steer" the regiospecific metabolism of other drugs. They further emphasize that ligands that yield apparent type II optical spectra are not necessarily directly ligated to the heme iron or necessarily inhibitory, as recently revealed by Jones and co-workers.[5,6]

Received: June 5, 2012
Revised: July 14, 2012
Published: July 18, 2012

dx.doi.org/10.1021/bi300744z | *Biochemistry* 2012, 51, 6441−6457

MATERIALS AND METHODS

Chemicals. 1*H*-1,2,3-Triazole, imidazole, 1*H*-1,2,4-triazole, and 17α-ethynylestradiol used during binding and turnover analysis were obtained from Sigma Chemical Co. (St. Louis, MO) and used without further purification. All reagents, purification solvents, and chemical precursors used during synthesis of 17-click, 2-OH 17-click, and 4-OH 17-click were also obtained from Sigma. Deuterated solvents for NMR analysis were purchased from Cambridge Isotopes (Andover, MA). Solvents for liquid chromatography and mass spectrometry (LC−MS) were of Optima grade from Fisher. Water not employed as LC−MS solvent was of Milli-Q quality from a Barnstead nanopure UV dispenser. Supersomes coexpressing cytochrome b_5 and P450 reductase were purchased from BD Biosciences (San Jose, CA).

^{1}H NMR. Characterization of synthesized 17-click, 2-OH 17-click, and 4-OH 17-click by NMR was performed on a Varian (Palo Alto, CA) Inova 500 (500 MHz) spectrometer equipped with a 5 mm HCN *z*-axis PFG triple-resonance probe.

Protein Expression and Purification. CYP3A4 was expressed and purified as previously described.[12] CYP2C9 (hepta mutant) was constructed as previously described[13] with the exeption of a hexa-His rather than a tetra-His C-terminal sequence to facilitate purification. The enzyme was expressed in *Escherichia coli* DL39 and purified as described for CYP3A4.

Synthesis of 17α-(2*H*-2,3,4-Triazolyl)estradiol (17-click). 17α-(2*H*-2,3,4-Triazolyl)estradiol (**1**) was obtained using a one-step click reaction between 17-α-ethynylestradiol and azidotrimethylsilane using a published procedure for preparation of N-unsubstituted 1,2,3-triazoles.[14] Purification was achieved using silica gel (0.035−0.07 mm, 6 nm pore diameter) chromatography with 8% CH_3OH in CH_2Cl_2 isochratic mobile phase to afford pure **1** in 60% yield: NMR (DMSO-d_6) δ 0.93 (3H, s, 18-CH_3), 6.40 (1H, d, J = 2.4 Hz, 4-H), 6.46 (1H, dd, J = 8.4, 2.4 Hz, 2-H), 6.95 (1H, d, J = 8.4 Hz, 1H), 8.95 (1H, s, triazole -CH), 14.69 (1H, broad s, triazole -NH); MS [M + H] (theoretical) 340.203, [M + H] (observed) 340.202.

Synthesis of 2-OH and 4-OH 17-Click. 19-Nor-17α-pregna-1,3,5(10)-trien-20-yne-2,3,17β-triol (**2**) and 19-nor-17α-pregna-1,3,5(10)-trien-20-yne-3,4,17β-triol (**3**) were synthesized using the protocol of Xie et al.[15] with minor modifications. Notably, during electrophilic aromatic substitution (formylation reaction, step 1), the Grignard reagent, EtMgBr, was used as a 1 M solution in THF delivered to the reaction after 1:6 dilution in anhydrous diethyl ether. For successful acylation reaction, triethyl phosphate was used as suggested. It was observed during the Dakin oxidation (step 2) that the molar ratio of NaOH and H_2O_2 is critical to limiting the formation of unwanted byproducts. Therefore, standardized 1 M NaOH (0.75 equiv) and 3% H_2O_2 (1.1 equiv; ε_{240} = 43.6 M^{-1} cm^{-1} [16]) solutions were prepared and added to an argon-purged THF solution of the 2-formyl and 4-formyl intermediates for a final aqueous concentration of 8.6% (v/v). The catechol products were separated on silica gel (0.035−0.07 mm, 6 nm pore diameter) with 2% CH_3OH in CH_2Cl_2 mobile phase under isocratic conditions. **2** was isolated in 48% overall yield and **3** in 8% overall yield; both were off-white solids. NMR chemical shifts and MS data for all intermediates conformed to that published previously.[15] To generate 2-OH 17-click (**4**) and 4-OH 17-click (**5**), click reactions were conducted in microscale using a procedure slightly modified from that used to obtain **1**. To a small conical pressure vial was added 400 μL of a DMF/H_2O (4:1) solution containing 11 mg (35 μmol) of intermediate **2** or **3**, followed by addition of 7 mg of sodium ascorbate (35 μmol) and 1 mg of $CuSO_4{\cdot}5H_2O$ [4 μmol of Cu(II)]. The solution was purged with argon while being stirred at room temperature before initiation of the reaction with 7.5 μL (57 μmol) of azidotrimethylsilane. The reaction mixture was heated (100 °C) overnight with vigorous stirring. The mixture was diluted with water prior to extraction with ethyl acetate. The organic layer was washed with several equivalents of water prior to treatment with brine and anhydrous $MgSO_4$. The organic layer was evaporated to dryness and the residue purified over silica gel (70−230 mesh, 100 Å pore) using a 5 in. disposable glass pipet with a 5−8% CH_3OH in CH_2Cl_2 mobile phase. Both **4** and **5** were isolated as slightly yellow solids in ∼30% yield. **4**: NMR (CD_3OD) δ 1.05 (3H, s, 18-CH_3), 6.43 (1H, s, 4-H), 6.61 (1H, s, 1-H), 7.65 (1H, broad s, triazole -CH); MS [M + H] (theoretical) 356.197, [M + H] (observed) 356.196. **5**: NMR (CD_3OD) δ 1.05 (3H, s, 18-CH_3), 6.53 (1H, d, J = 8.8 Hz, 2-H), 6.55 (1H, d, J = 8.8 Hz, 1-H), 7.64 (1H, broad s, triazole -CH); MS [M + H] (theoretical) 356.197, [M + H] (observed) 356.197.

Kinetic Assay. Kinetic parameters k_{cat} and K_M for total 17-click turnover were estimated by LC−MS/MS using the methods of substrate depletion.[17,18] Briefly, typical incubation mixtures were prepared by combining 198 pmol of rCYP3A4 in Supersomes coexpressing P450 reductase and cytochrome b_5 (198 μL, working P450 concentration of 50 nM based on 0.5 nmol of P450/0.5 mL as determined by the manufacturer), 79.2 μL of an appropriate 50× 17-click stock solution (0.005−10 mM) in ethanol [final EtOH concentration of 2% (v/v)], and 3286.8 μL of KP_i (0.1 M, pH 7.4; 6 mM $MgCl_2$) buffer. Triplicate 90 μL aliquots were dispensed in 96-well plate format prior to preincubation of the plates at 37 °C for 5 min. Wells representing the time zero point received 10 μL of KP_i buffer, while the reactions were initiated by addition of 10 μL of a 10 mM NADPH solution (final concentration of 1 mM). Reactions were quenched every 30 s up to 3.5 min, and then every 1−2 min up to 16 min with 150 μL of acetonitrile containing 1 μM carbamazapine (CBZ) as an internal standard (IS). The quenched reactions were centrifuged at 3480*g* and 4 °C for 10 min to remove precipitated protein. LC−MS/MS analysis of the samples was conducted on an API 4000 triple quadrupole mass spectrometer in positive electrospray mode (MDS SCIEX, Concord, ON), coupled to LC-10ADvp pumps and a SCL-10ADvp controller (Shimadzu, Columbia, MD) with a CTC PAL (Leap Technologies, Carrboro, NC) autosampler. For LC, an Aquasil (Thermo Scientific) C18, 30 mm × 2.1 mm (inside diameter) (3 μm pore size) column was used with water (solvent A) and acetonitrile (solvent B) mobile phases containing 0.1% formic acid. Data were acquired in multiple-reaction monitoring (MRM) scan mode monitoring the transitions m/z 340.2/159.1 (Q1/Q3) for the 17-click parent and m/z 237.2/193.1 (Q1/Q3) for the CBZ internal standard. The desolvation temperature was 650 °C, the spray voltage 2.5 kV, the declustering potential 55 V, the collision energy 38 V, the entrance potential 10 V, and the exit potential 13 V. Data analysis was conducted with analyte:IS peak area ratios determined using Analyst (AB SCIEX, Framingham, MA) as described previously.[17]

Incubation mixtures for measurement of 17EE depletion were prepared in a fashion identical to that described for 17-click. 17EE reactions were quenched every 30 s (up to 4 min)

with 200 μL of ethyl acetate containing 0.1 μM β-estradiol IS. The quenched plates were placed in a dry ice/acetone bath to separate the aqueous layer, and the organic layer was removed and evaporated to dryness in a new plate under a gentle stream of nitrogen at 45 °C. To facilitate detection of 17EE by ESI-MS/MS, the reaction residue was resuspended in 100 μL of 50 mM sodium carbonate buffer (pH 11.0) and 100 μL of 1 mg/mL dansyl chloride in an acetone solution. The derivatization reaction mixtures were heated (50 °C) for up to 40 min. The derivatized reaction mixtures were assayed directly by MRM after automatic tune optimization with infused standards in positive ion mode: m/z 530.4/171.1 (Q1/Q3) to detect parent 17EE and m/z 506.4/171.1 (Q1/Q3) for β-estradiol IS.

Measurement of the 17-Click IC_{50}. The median inhibitory concentrations (IC_{50}) of 17-click were determined against testosterone 6β-hydroxylation by CYP3A4 in Supersomes coexpressing P450 reductase and cytochrome b_5. Incubations in 100 mM KP_i (pH 7.4) contained varying concentrations of 17-click (0−60 μM), 10 nM enzyme, and 50 μM testosterone and were preincubated for 5 min prior to initiation of the reaction with NADPH (10 mM, final concentration of 1 mM). Triplicate reactions were quenched after 20 min using an equal volume (100 μL) of 1 μM tolbutamide (IS) in acetonitrile. Quantitation of the percent remaining activity was conducted using the MRM scan mode of a 4000Q-Trap (MDS SCIEX) connected to a Shimadzu HPLC system. 6β-Hydroxytestosterone was monitored using m/z 305.0 and 269.0 (Q1/Q3) with a declustering potential of 55 and a collision energy of 25. Tolbutamide was monitored using m/z 271.2 and 91.1 (Q1/Q3), using a declustering potential of 66 and a collision energy of 39. The following instrument settings were applied: dwell time, 500 ms; curtain gas, 10; spray voltage, 4.5 kV; source, 400 °C; ion spray gas 1 and 2, 40.

HPLC−qTOF MS Analysis of 17-Click Metabolites. Liquid chromatography was performed using a Waters (Milford, MA) ACQUITY UPLC system coupled to a SYNAPT High Resolution Quadrupole TOF mass spectrometer via an ESI interface. Chromatographic separation was achieved on a Hypersil GOLD (ThermoFisher) UPLC column (150 mm × 2.1 mm, 1.9 μm particle size). A gradient program consisting of solvent A [H_2O containing 0.1% formic acid (v/v)] and solvent B [ACN containing 0.1% (v/v) formic acid] was used. Solvent A was held at 90% for 3 min, followed by a linear gradient to 48% B over 12 min. Solvent B was then increased using a linear gradient to 95% B at 17 min and held for 5 min. Pre-equilibration of the column at 90% A was conducted for 5 min prior to each injection. The parent ions were detected in full scan mode (m/z 50−800) with a cone voltage of 17 eV, a collision energy of 6 eV, and a transfer cell energy of 4 eV. For fragmentation analysis, data were aquired in MS expression (MS^E) mode, with the cone voltage set to 17 eV, the collision cell set to 4 eV, and the trap cell set to 6 eV. Fragmentation in the MS^E mode was induced using a collision energy ramp of 15−45 eV. In both modes, the capillary voltage was set to 3.5 kV with a source temperature of 120 °C and desolvation temperature of 350 °C. Calibration of the instrument was performed using sodium formate over a range of 50−800 prior to use. Leucine enkephalin was used as a lockspray reference with a sampling interval of 30 s and a scan rate of 1.0 s. Spectra were averaged for the fwhm of the metabolite peaks using Masslynx and subjected to mass defect filtering with Metabolynx using a parent mass tolerance of 50 mDa. All elemental compositions were determined using Masslynx. The Masslynx software MassFragment was used to obtain structural proposals for the fragments.

Ion Trap LC−MS^n Analysis of 17-Click Metabolites. Further characterization of the primary 17-click metabolite (M4) was conducted using a Finnigan LTQ ion trap instrument (Thermo Electron Corp., San Jose, CA) connected to an Agilent 1100 series HPLC system equipped with an auto-injector. Ionization of the metabolites was achieved by ESI in the positive ion mode. The capillary temperature was 300 °C, the sheath gas flow 40, the auxiliary gas flow 10, and the source voltage 3 kV. MS^4 was conducted using two distinct normalized collision energy sequences: (1) m/z 356 @ 8%, m/z 338 @ 15%, and m/z 213 @ 20% and (2) m/z 356 @ 8%, m/z 338 @ 15%, and m/z 320 @ 20%. An activation time of 30 ms was used throughout both sequences. LC conditions were as described above for qTOF analysis.

Computational Methods. Density functional theory (DFT) calculations were performed on a simplified heme macrocycle consisting of an unsubstituted porphine, ferric iron, thiolate (-SH) proximal ligand complex with a variable neutral sixth distal ligand (e.g., water, IMZ, 1,2,3-TRZ, or 1,2,4-TRZ). Structures were initially built in Avogadro. DFT calculations were performed with GAMESS [version 1, October 2010 (R1)]. Calculations used unrestricted DFT (M06) methods.[19] We set the charge of the molecule to zero; Fe(III) with balancing negative charges on the macrocycle (−2) and thiolate (−1); and the Fe(III) spin (S) to be $^1/_2$, corresponding to a single unpaired electronic configuration. GAMESS-implemented DFT used a Euler−Maclaurin quadrature with 96 radial points, with θ and ϕ set to 12 and 24, respectively, for the number of angle grids in the Gauss−Legendre quadrature. The molecular coordinates used were systematically generated delocalized internal coordinates generated from Cartesian coordinates in the GAMESS input file. Basis sets for geometry optimization and energy calculations were s6-31G(d),[20] implemented as spherical harmonics unless indicated otherwise. Convergence criteria were loosened in all heme calculations. All calculation parameters used GAMESS default settings unless otherwise mentioned. GAMESS output was visualized using MacMolPlt.[21] The relative binding energy of the fragment azoles was evaluated in silico by assessing the equilibrium between the resting state heme complex [Fe(III)−H_2O] and the free azole fragment on the reactant side of the equilibrium and azole-bound heme [Fe(III)−azole] and free H_2O on the product side of the equilibrium. The differences in the sum of energies on the product and reactant side were used to calculate $\Delta E_{binding}$ for each azole fragment, which corresponds to the difference in energy between the water-ligated and azole-ligated model heme. Bond orders were calculated using Mullikan population analysis of the canonical Kohn−Sham orbitals.

UV−Vis Absorbance Analysis of Ligand Binding. Absorbance measurements were conducted on an Olis Modernized Aminco DW-2 (Olis, Inc., Bogart, GA) dual-beam spectrophotometer equipped with a Julabo F30-C compact refrigerated circulator (Julabo USA, Inc., Allentown, PA). Each binding experiment required a 500 μL initial sample volume using a 0.1 cm × 1 cm path length quartz cuvette, and the typical sample consisted of 1−2 μM purified CYP in 100 mM KP_i buffer with 20% glycerol. Spectra were recorded in the absolute mode (270−650 nm) between 1 μL aliquots of the appropriate ligand stock solution added to the sample cuvette. For titrations of lipophilic species 17EE and 17-click, ethanol stock solutions were used with a final concentration of organic

dx.doi.org/10.1021/bi300744z | Biochemistry 2012, 51, 6441−6457

kept below 2% (v/v). During temperature-dependent measurements (van 't Hoff analysis), the protein samples were allowed to equilibrate at the desired temperature for a minimum of 10 min prior to initiation of the experiment, and the sample was allowed to equilibrate for 5 min between ligand aliquots prior to data acquisition. The temperature was precisely monitored inside the cuvette by thermocouple, and fluctuations larger than ±0.4 °C during the course of the experiment resulted in a discarding of the data. Corrections were applied to the data to account for baseline drift and sample dilution over the course of the binding experiments. Difference spectra were generated by subtracting the ligand-free spectrum from all ligand-containing spectra, and binding isotherms were constructed using the spectral peak minus spectral trough intensity values plotted as a function of ligand concentration. Affinity, K_D, and B_{max} parameters were estimated from nonlinear regression analysis in IGOR pro 6.1 (Wavemetrics, Lake Oswego, OR) using eq 1. Equations 2–4 were used when curvature was observed in the Eadie–Hofstee transform of the data.

$$\Delta\text{Abs} = [\text{E}\cdot\text{L}] = (B_{max}[\text{L}])/(K_D + [\text{L}]) \quad (1)$$

$$\Delta\text{Abs} = [\text{E}\cdot\text{L}] = (B_{max}[\text{L}]^n)/(K_s{}^n + [\text{L}]^n) \quad (2)$$

$$\Delta\text{Abs} = [\text{E}\cdot\text{L}] = (B_{max,1}[\text{L}])/(K_{D1} + [\text{L}]) + (B_{max,2}[\text{L}])/(K_{D2} + [\text{L}]) \quad (3)$$

$$\Delta\text{Abs} = [\text{E}\cdot\text{L}] = [(B_{max,1}[\text{L}])/K_{D1} + (B_{max,2}[\text{L}]^2)/(K_{D1}\cdot K_{D2})]/[1 + [\text{L}]/K_{D1} + [\text{L}]^2/(K_{D1}\cdot K_{D2})] \quad (4)$$

To accurately compare UV–vis binding spectral characteristics for azole fragments and for 17-click, the spectra for a given titration were normalized to a CYP concentration of 1 μM using the Soret band absorbance measured in the absence of ligand (CYP3A4 ε_{417} = 115 mM^{-1} cm^{-1};[22] estimated for CYP2C9 $\varepsilon_{417} \sim 133$ mM^{-1} cm^{-1}). For CYP3A4 binding spectra, comparison of trough intensity at 390 nm in calculated difference spectra was used as an estimate of type IIa character.[23,24] In cases where complete saturation had not been achieved at the highest experimental ligand concentration, principal component analysis (PCA) was conducted as described previously[25−27] using software written in the Python programming language (version 2.6) and adapted to IGOR Pro 6.1 (Wavemetrics, Lake Oswego, OR) to yield the "saturated" type II binding spectrum and facilitate more accurate spectral comparisons.

van 't Hoff Data Analysis. The natural logarithm of the equilibrium association constant ($\ln K_a = \ln K_D{}^{-1}$) obtained by nonlinear regression analysis of the UV–vis-generated binding isotherms was plotted as a function of inverse experimental temperature (kelvin). At each temperature, K_a was measured in duplicate and the associated standard error from the fit was assigned to each point in the van 't Hoff plot to be weighted during regression analysis using the linear form of the van 't Hoff equation: $\ln K_a = -\Delta H°/R(1/T) + \Delta S°/R$. $\Delta H°$ and $\Delta S°$ were calculated from the best fit slope and intercept, respectively, using an R value of 1.9859 cal mol^{-1} K^{-1}.

Corrections to IMZ Concentration during van 't Hoff Analysis. Because of the mixture of charge states anticipated at pH 7.4 for basic IMZ, a correction procedure was applied to the absolute IMZ concentration when determining K_a and is based on several assumptions. (1) Only the neutral fraction of the IMZ fragment is involved in CYP binding. (2) The temperature dependence of pK_a for the IMZ ionization reaction is accurately described by published values for the thermodynamic parameters $\Delta H°$ and $\Delta C_p°$ measured under dilute aqueous conditions.[28] (3) The IMZ·H^+ activity coefficient ($\gamma_{IMZ\cdot H^+}$) can be calculated at a constant ionic strength determined by the buffer ($I \approx 240$ mM KP_i) without accounting for short-range nonelectrostatic interactions using the extended Debye–Hückel expression (eq 5)

$$\ln \gamma i = -A_m z_i{}^2 I^{1/2}/(1 + BI^{1/2}) \quad (5)$$

where A_m represents the Debye–Hückel constant (temperature-dependent values between 0.494 and 0.513 $kg^{1/2}$ $mol^{-1/2}$ taken from ref 29), z_i the charge of the ith ion, I the ionic strength of the solution, and B the so-called "ion size" parameter (set equal to 1.6 $kg^{1/2}$ $mol^{-1/2}$ as described in ref 30). First, published values (pK_{a298K} = 7.09 ± 0.1, $\Delta H°$ = 36.59 ± 0.06 kJ/mol, and $\Delta C_p°$ = −16 ± 5 J mol^{-1} K^{-1}), reported in the study by Fukawa and Takahashi[28] for the IMZ proton dissociation reaction (K_a) occurring in the presence of 100 mM potassium chloride, were used to calculate pK_a within the range of experimental temperatures used in this study via the methods of Clarke and Glew (eq 6).[31]

$$\log K(T) = \log K°_{298} + \Delta H°_{298}/R \times \ln 10(1/298 - 1/T) + \Delta C_p°{}_{298}/R \times \ln 10[298/T + \ln(T/298) - 1] \quad (6)$$

From the expression ($10^{pH-pK_a} \times \gamma_{IMZ\cdot H^+}$) = [IMZ]/[IMZ·$H^+$], the molar IMZ fraction was obtained using calculated values for pK_a and $\gamma_{IMZ\cdot H^+}$, along with the initial measured buffer pH. The IMZ concentrations were then corrected accordingly prior to nonlinear regression analysis of the binding isotherms to estimate IMZ affinity (K_D). It was observed that addition of up to 6 mM IMZ to the buffered solutions only minimally affected the final solution pH (+0.03 unit). It is noted that ionic strength corrections to $\Delta H°$ and $\Delta C_p°$ parameters describing deprotonation reactions for charge symmetric systems, such as the case of the deprotonation of amines, are zero at this level of theory.[30]

Pulsed CW EPR. EPR measurements were conducted at X-band on an ELEXSYS E680 EPR spectrometer (Bruker-Biospin, Billerica, MA) equipped with a Flexline ER 4118 CF cryostat and a Flexline ER 4118X-MD4 ENDOR resonator. A two-dimensional pulsed EPR technique, HYSCORE, was used to probe the interaction of nearby nuclei. A $\pi/2-\tau-\pi/2-t_1-\pi-t_2-\pi/2-\tau-$echo pulse sequence in which τ, t_1, and t_2 indicate delays between pulses whose nominal turning angles are $\pi/2$ or π was used. A 16-step phase cycle was used to reject unwanted responses and correct the baseline as explained in ref 32. In HYSCORE, ENDOR frequencies (the hyperfine-shifted NMR frequencies) from nuclei in the vicinity of the unpaired electron spin are correlated with each other and dispersed in two dimensions, allowing resolution of the peaks that overlap in simple one-dimensional spectra. HYSCORE spectra were collected at the g_z (low-field) peak of the EPR spectrum. HYSCORE spectra from protons were analyzed using the contour line shape analysis[33,34] followed by complete spectral simulation with orientation selection.

Conventional continuous-wave (CW) EPR spectra were measured on a Bruker ELEXSYS E540 X-band spectrometer with an ER 4102 ST resonator and either a liquid nitrogen quartz insertion dewar or a Bruker ER 4112 HV helium flow cryostat. EPR samples were prepared by mixing 50 μL of a protein solution containing 20% glycerol with 225 μM 17-click and 50 mM 1*H*-1,2,3-triazole. These samples were placed in 3 mm outside diameter EPR tubes, frozen, and stored in liquid nitrogen. The spectral *g* values were obtained by fitting the CW EPR spectra using Easyspin.[35]

RESULTS

Models for Type II CYP Binding: 1,2,3-TRZ−Heme Energetics Calculated by DFT. Gas phase DFT calculations [s6-31G(d) basis set, U-M06 functional[19,20,36]] were conducted to examine the binding of a model Fe(III) heme with 1,2,3-TRZ, 1,2,4-TRZ, and IMZ fragments to assess the potential for 1,2,3-TRZ-based ligands to form type II complexes with CYPs (Table 1). The M06 functional was chosen, in part, because it has been parametrized using transition metals in the training set and correctly predicts the Fe−azole versus Fe−H_2O bond energies, whereas the popular B3LYP hybrid functional fails (data not shown).[19] This nonisodesmic comparison is necessary because the resting state of the enzyme is six-coordinate with water as the distal axial ligand, although the isodesmic comparisons within the different N−Fe cases should show better correlation with experiment. All computational comparisons are isogyric as the water-ligated and azole-ligated heme structures are both low-spin forms with *S* values of $^1/_2$. The energies for the gas phase reaction between H_2O-ligated low-spin model heme-thiolate and the free azole fragments (Materials and Methods) are listed in Table 1: IMZ (−5.3 kcal/mol) > 1,2,4-TRZ (−3.2 kcal/mol) > 1,2,3-TRZ (−1.7 kcal/mol). This result suggests that 1,2,3-TRZ−heme interactions are slightly weaker energetically than the other azole complexes but still favorable relative to those of the H_2O-ligated state. Our results correlate with the solution pK_a of the fragments [6.99 (IMZ) > 2.45 (1,2,4-TRZ) > 1.15 (1,2,3-TRZ)],[37] suggesting basicity is a major determinant for heme coordination. Thus, 1,2,3-TRZ was anticipated to induce similar type II optical signatures in CYP, albeit with a lower affinity (K_D) than IMZ and 1,2,4-TRZ. Interestingly, interactions with the heme of both N1 and N2 of 1,2,3-TRZ are comparable.

Table 1. Results of Gas Phase DFT Calculations[a]

	ΔE_{rxn} (kcal/mol)	bond order	bond length (Å)
IMZ	−5.3	0.311	2.081
1,2,4-TRZ	−3.2	0.285	2.088
1,2,3-TRZ (N1)	−1.7	0.258	2.101
1,2,3-TRZ (N2)	−2.8	0.248	2.093

[a]s6-31G(d) basis set, U-M06 functional.

Apparent Type II Binding of the 1,2,3-TRZ Fragment to Multiple CYPs. Despite the DFT results, which indicate that 1,2,3-TRZs could interact with heme, an extensive analysis of the literature revealed no CYP-targeted azole drugs that possess the fragment. Therefore, we explored experimentally the possibility that 1,2,3-TRZ can form type II complexes, and how these complexes compare spectrally with established druglike azole fragments, 1,2,4-TRZ, and IMZ. Two mammalian CYP isoforms, CYP3A4 and a CYP2C9 variant (N-terminal truncation and hepta mutant,[13] CYP2C9dh; hereafter termed CYP2C9), were expressed and purified.[13,38] Figures 1 and 2 display the calculated difference spectra and resultant binding isotherms obtained from UV−vis absorbance titration of CYP3A4 and CYP2C9, respectively, with 1,2,3-TRZ, 1,2,4-TRZ, and IMZ at 20 °C in 100 mM KP_i (pH 7.4, 20% glycerol). The pertinent spectral features of each titration are summarized in Table 2. All three fragments yield type II spectral complexes, which suggest that they displace the axial water molecule from resting state heme and coordinate to ferric iron.[39] The magnitude of the Soret band red shift varies in CYP3A4 [IMZ (8 nm) > 1,2,4-TRZ (6 nm) = 1,2,3-TRZ (6 nm)], with similar shifts observed in the α/β region. In CYP2C9, the Soret shifts vary [IMZ (9 nm) > 1,2,4-TRZ (5 nm) > 1,2,3-TRZ (2 nm)], with similar shifts in the α/β spectral region. The affinity was markedly lower for the 1,2,3-TRZ fragment binding both CYP3A4 [K_D = 14.3 ± 0.5 mM; ∼38-fold lower vs IMZ and up to ∼367-fold lower vs 1,2,4-TRZ (Table 2)] and CYP2C9 [K_D = 10.0 ± 0.4 mM; up to ∼50-fold lower vs 1,2,4-TRZ and ∼101-fold lower vs IMZ (Table 2)]. Curiously, these results corroborate a previous report[23] of complexity inherent in the binding of 1,2,4-TRZ to CYP3A4 and CYP2C9, which manifests as pronounced curvature in Eadie−Hofstee plots (Figures 1 and 2, inset). In both cases, the data fit best to a two-site binding model (Materials and Methods, eq 4): the first molecule of 1,2,4-TRZ binds CYP3A4 with a K_{D1} of 0.039 ± 0.007 mM and is responsible for 13% of the total absorbance change observed at saturation, followed by binding of a second low-affinity equivalent with a K_{D2} of 4.80 ± 0.21 mM; in CYP2C9, both 1,2,4-TRZ binding sites are responsible for nearly equal shifts toward the low-spin azole-ligated spectrum (51 and 49% total spectral shifts at saturation for high-affinity and low-affinity sites, respectively), and the first molecule of 1,2,4-TRZ binds with a K_{D1} of 0.198 ± 0.040 mM followed by a second low-affinity equivalent with a K_{D2} of 2.85 ± 0.82 mM. In contrast to a previous report,[23] multiple bindings of IMZ were not observed in our titrations with CYP2C9. Possibly, the difference lies in the use of the wild-type enzyme versus the variant used in our studies.

Regardless of these system-dependent differences, the binding studies and DFT calculations demonstrate that type II binding is favorable in the case of 1,2,3-TRZ. The DFT calculations correctly predict the rank order affinity of the three ligands for CYP2C9, but they fail to correctly predict the rank order affinity for CYP3A4 binding (1,2,4-TRZ > IMZ > 1,2,3-TRZ). This is not an altogether surprising result, as the DFT calculations do not include zero-point energy, solvent interactions, or the possible contribution of the protein itself to binding free energies.

Comparative van 't Hoff Analysis of Binding of 1,2,3-TRZ and IMZ to CYP3A4. The thermodynamic basis for the inferior CYP3A4 binding energetics of 1,2,3-TRZ relative to those of IMZ was investigated by van 't Hoff analysis to estimate $\Delta H°_{binding}$ and $\Delta S°_{binding}$. 1,2,4-TRZ was excluded from the analysis because of the additional binding complexity observed during the initial binding screen. The temperature dependence of the equilibrium association constant (K_a) for binding of azole to CYP3A4 was measured via UV−vis absorbance titration within a temperature range of 5−30 °C in 100 mM KP_i (pH 7.4, 20% glycerol), and the results are shown in Figure 3. To account for the relatively high basicity of IMZ and accurately define its thermodynamic quantities for CYP binding, we used an additional correction procedure

dx.doi.org/10.1021/bi300744z | *Biochemistry* 2012, 51, 6441−6457

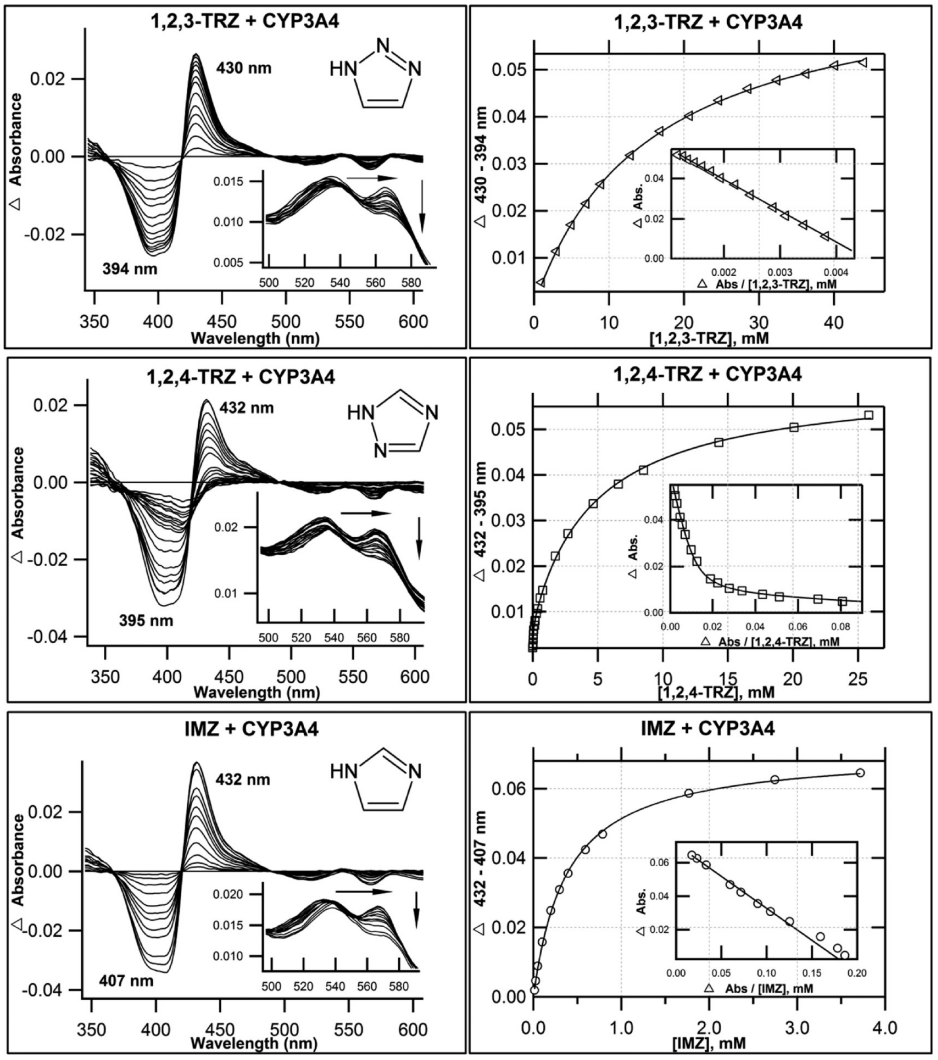

Figure 1. Optical titrations and binding isotherms for nitrogen heterocycles binding to CYP3A4. 1,2,3-TRZ binding CYP3A4 shows type II behavior. UV−vis equilibrium absorbance titration (20 °C) of purified CYP3A4 (1−2 μM, 0.1 M KP_i, pH 7.4, 20% glycerol) with 1,2,3-TRZ (top), 1,2,4-TRZ (middle), and IMZ (bottom). Shown are calculated difference spectra (left), with the α and β region of the recorded absolute spectra as insets, and the resultant binding isotherms (right), generated by plotting Δ(peak − trough) intensities as a function of ligand concentration, with best fits used to estimate K_D (Table 2). Interestingly, 1,2,4-TRZ displays complex equilibrium binding behavior (see the text) that is most evident as curvature in the Eadie−Hofstee transform (inset), shown here fit to a two-site binding model (Materials and Methods, eq 4).

(Materials and Methods) to calculate the effective IMZ concentration present during binding analysis, with the assumption that only neutral IMZ species binds CYP. Similar corrections were unnecessary for 1,2,3-TRZ because it is expected to exist in essentially 100% neutral form at pH 7.4 (pK_a = 1.15[37]). From the fits to the linear form of the van 't Hoff equation (Materials and Methods), estimates of $\Delta H^\circ_{binding}$ and $\Delta S^\circ_{binding}$ for both species were calculated from the slope and y-intercept, respectively. In 100 mM KP_i, binding of both fragments is enthalpically favorable, as would be expected for azole fragments that directly coordinate heme iron and presumably make little or no contact with active site residues. Values of $\Delta H^\circ_{binding}$ were similar for IMZ (−8.1 ± 0.3 kcal/mol) and 1,2,3-TRZ (−8.8 ± 0.1 kcal/mol), clearly demonstrating that the main determinant for the low $\Delta G^\circ_{binding}$ for 1,2,3-TRZ relative to IMZ is entropy, which is much more unfavorable for 1,2,3-TRZ ($\Delta S^\circ_{binding}$ = −22 ± 0.4 cal mol^{-1} K^{-1} for 1,2,3-TRZ; $\Delta S^\circ_{binding}$ = −10 ± 1 cal mol^{-1} K^{-1} for IMZ). It is suggested here that this discrepancy for $\Delta S^\circ_{binding}$ between IMZ and 1,2,3-TRZ may be due, in part, to the unusual nature of 1,2,3-TRZ tautomeric equilibria. Specifically, the well-documented dependencies of these equilibria on solvent polarity, solute concentration, and temperature[40] (see Discussion) suggest that protein binding and heme ligation may further influence the distribution of 1,2,3-TRZ tautomers, which have unique electronic properties such as differing dipole moments[41] and NMR chemical shifts.[40]

Influence of 1*H*-1,2,3-Triazole Fragment on CYP−Inhibitor/Substrate Interactions: The Case of 17α-Ethynylestradiol. *Equilibrium Binding.* The results mentioned above demonstrate the potential for the isolated 1,2,3-TRZ fragment to form a type II complex with multiple CYPs, albeit with lower affinity than other nitrogenous isosteres. Thus, it remains unclear whether the interactions between this fragment and the heme could be strong enough to influence binding of a well-characterized CYP3A4 substrate. To investigate this possibility, 17α-ethynylestradiol (17EE), a type I substrate/mechanism-based inhibitor was chosen for derivatization because of its well-characterized metabolic profile, which suggests the molecule prefers to dock with its

dx.doi.org/10.1021/bi300744z | *Biochemistry* 2012, 51, 6441−6457

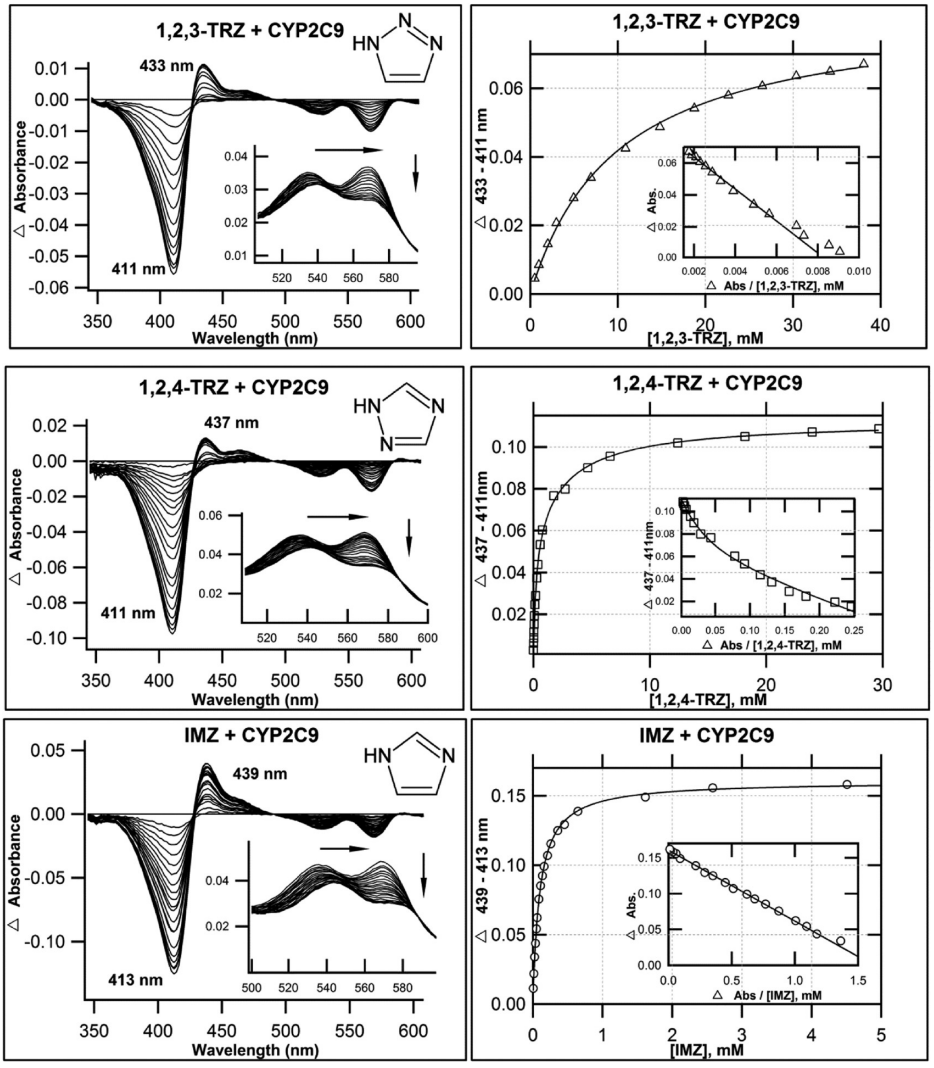

Figure 2. Optical titrations and binding isotherms for nitrogen heterocycles binding to CYP2C9. 1,2,3-TRZs binding to CYP2C9 yield type II behavior. UV−vis equilibrium absorbance titration (20 °C) of purified CYP2C9h (1−2 μM, 0.1 M KP_i pH 7.4, 20% glycerol) with 1,2,3-TRZ (top), 1,2,4-TRZ (middle), and IMZ (bottom). Shown are calculated difference spectra (left), with the α and β region of the recorded absolute spectra as insets, and the resultant binding isotherms (right), generated by plotting Δ(peak − trough) intensities as a function of ligand concentration, with best fits used to estimate K_D (Table 2). As with CYP3A4, 1,2,4-TRZ displays complex equilibrium binding to CYP2C9, which is most evident as curvature in the Eadie−Hofstee transforms (inset). The data fit best to a two-site model (Materials and Methods, eq 4) in which binding at each site induces similar spin shifts.

Table 2. UV−Vis Absorbance Data for the Azole Fragments Binding CYP3A4 and CYP2C9

	Soret (nm)	α (nm)	β (nm)	α:β	difference:peak (nm)	difference:trough (nm)	ΔAbs_{max} (1 μM)[b]	ΔAbs_{390} (1 μM)[c]	K_D (mM)
CYP3A4[a]	416	565	534	0.94	–	–	–	–	–
1,2,3-TRZ	422	565	538	0.77	430	394	0.058	−0.023	14.3 ± 0.5
1,2,4-TRZ	422	569	537	0.74	432	395	0.0065, 0.050	−0.025	K_{D1} = 0.0390 ± 0.0071, K_{D2} = 4.80 ± 0.22
IMZ	424	570	538	0.73	432	407	0.065	−0.027	0.381 ± 0.011
CYP2C9[a]	418	569	537	1.1	–	–	–	–	–
1,2,3-TRZ	420	570	540	0.84	433	411	0.041	–	10.0 ± 0.4
1,2,4-TRZ	423	572	542	0.78	437	411	0.023, 0.044	–	K_{D1} = 0.198 ± 0.040, K_{D2} = 2.85 ± 0.82
IMZ	427	574	544	0.77	439	413	0.066	–	0.0989 ± 0.0018

[a]At 20 °C. [b]Maximal peak trough intensity normalized to 1 μM. [c]Used as an estimate of efficiency of the type II ligand to decrease the inherent high-spin enzyme fraction (type IIa).[24]

steroid A-ring nearest heme (see Discussion) and thus provides an opportunity to test the energetics of 1,2,3-TRZ−heme interactions by installing the fragment on the opposing end (D-ring) of the core steroid structure. 17EE was successfully

dx.doi.org/10.1021/bi300744z | Biochemistry 2012, 51, 6441−6457

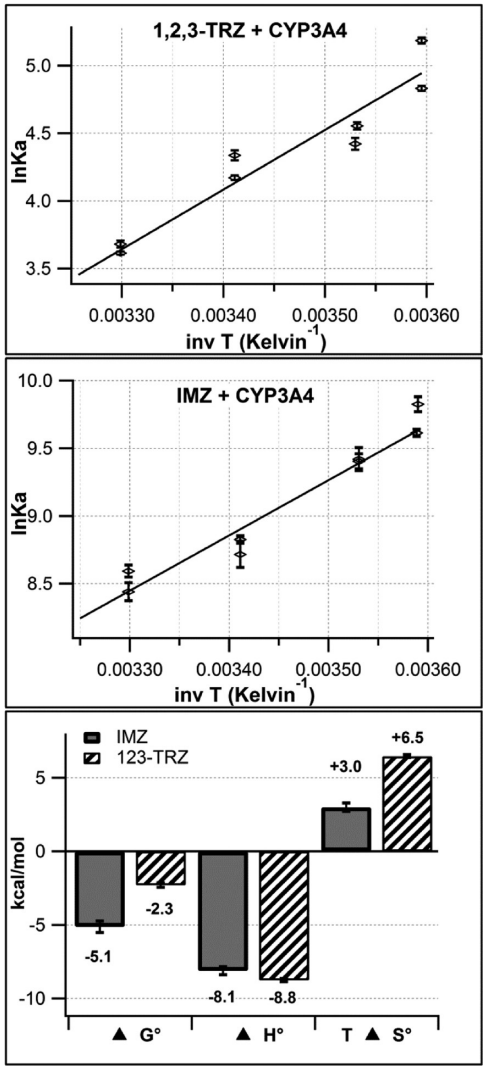

Figure 3. van 't Hoff plots demonstrating the temperature dependence (5−30 °C) of the equilibrium affinity constant (K_a) for binding of 1,2,3-TRZ (top) and IMZ (middle) to CYP3A4 (1 μM) in 100 mM KP_i (pH 7.4, 20% glycerol) as measured by UV−vis absorbance titration. Fit results provide estimates for $\Delta H°_{binding}$ and $\Delta S°_{binding}$ and are summarized in the bar graph (bottom) with values of $\Delta G°$ at 298 K. K_a values plotted for IMZ represent those obtained after correction of the IMZ titrant concentration to reflect only neutral species (see Materials and Methods).

derivatized to 17α-(2*H*-2,3,4-triazolyl)estradiol (17-click) and isolated in 60% yield using a one-step click reaction (Materials and Methods). Equilibrium binding of 17EE and 17-click to purified CYP3A4 in 100 mM KP_i (pH 7.4, 20% glycerol) were measured by UV−vis absorbance at 25 °C (Figure 4). 17EE binding induced a type I spectrum, typical of efficiently oxidized CYP substrates that are thought to displace the water molecule at the sixth axial position and favor the high-spin enzyme species.[39] The calculated 17EE binding isotherm displayed obvious sigmoidal behavior that is corroborated by pronounced curvature observed in an Eadie−Hofstee transformation of the data (not shown), suggesting the stoichiometry of binding is greater than unity (Figure 4). A simple Hill plot (not shown) was used for nonlinear regression analysis and exhibited a K_s of 37.7 ± 1.7 μM and a Hill coefficient of 1.75. The 17EE binding data were also fit to a two-site sequential binding model (Figure 4) (Materials and Methods, eq 4), and the best fit yielded a K_{D1} of 50 ± 25 μM for the first 17EE equivalent, which did not induce a significant heme spin state change, followed by binding of a second equivalent that perturbs the spin state with a K_{D2} of 19 ± 8 μM. This was not entirely unexpected, as similar CYP3A4−steroid spin-silent binding interactions have already been documented in our lab for testosterone[42] and are suggested by crystallographic results with progesterone bound to CYP3A4 at a peripheral site.[43]

In contrast, binding of 17-click to CYP3A4 displays a dramatic reversal of the spin state toward low-spin heme, as evidenced by the type II difference spectrum shown in Figure 4. This result suggests that despite the inferior azole−heme binding energetics of 1,2,3-TRZ compared with those of similar azole heterocycles IMZ and 1,2,4-TRZ, the 1,2,3-TRZ fragment is still capable of weighting the preferred 17EE binding poses to accommodate an additional type II binding interaction with heme iron. 17-Click binding was best described using a hyperbolic binding model with a K_D of 45.8 ± 3.1 μM. Interestingly, further inspection of the type II optical signature at near protein saturation reveals that the interaction may be "strained" or "incomplete" (Table 3). This assessment is based on the submaximal Soret red shift (2 nm) and decrease in the CYP3A4 high-spin fraction (ΔAbs_{390}) observed in the absolute absorbance spectrum, and most evident in the diminished peak to trough intensity difference observed in the calculated difference spectrum relative to what is observed for the 1,2,3-TRZ−heme complex. Others have suggested that UV−vis absorbance spectra for azole fragment−CYP complexes can be useful references for detecting suboptimal heme ligation for type II species bearing similar fragments.[23]

Structural Analysis of the CYP3A4−17-Click Low-Spin Complex by CW EPR and HYSCORE Spectroscopy. On the basis of DFT calculations and equilibrium binding studies conducted here, 1,2,3-TRZ fragment−heme interactions are anticipated to be weaker than imidazole−heme and 1,2,4-TRZ−heme interactions, but sufficient to modulate substrate orientation, at least in the case of 17-click. However, the incomplete spectral conversion with 17-click, compared to the larger spin state conversion with fragment 1,2,3-TRZ, suggested the possibility that the heme ligation is not complete in the former case. Speculatively, the incomplete difference spectrum described above for 17-click could be due to conformational heterogeneity or axial ligand heterogeneity on the heme.

Therefore, to test this hypothesis, CW and pulsed EPR techniques were used to examine the type II CYP3A4 complexes of 1,2,3-TRZ and 17-click. For these experiments, the concentration of KP_i was increased to 200 mM to achieve the high CYP3A4 concentration necessary for detectable EPR signals. The binding affinity of 17-click was demonstrated to be minimally affected by this change in ionic strength ($K_{D100\ mM}$ = 46 μM, and $K_{D200\ mM}$ = 78 μM), and the UV−vis absorbance spectra at saturation were identical to that observed previously (data not shown). Figure 5 shows the CW EPR spectra for ligand-free CYP3A4 and CYP3A4 with 1,2,3-TRZ and 17-click. The EPR spectra for ligand-free CYP3A4 have *g* values of 2.421 (g_z), 2.249 (g_y), and 1.921 (g_x). 1,2,3-TRZ shifted the EPR *g* values of this complex, with two unique sets identified by fitting the CW EPR spectrum (Materials and Methods): 2.505 (g_z), 2.259 (g_y), and 1.874 (g_x); and 2.459 (g_z), 2.261 (g_y), and 1.890 (g_x). Both species of 1,2,3-TRZ-bound CYP3A4 detected from the fit of the data have larger g_z values than the ligand-free enzyme. It is suggested here that two unique sets of *g* values for

dx.doi.org/10.1021/bi300744z | *Biochemistry* 2012, 51, 6441−6457

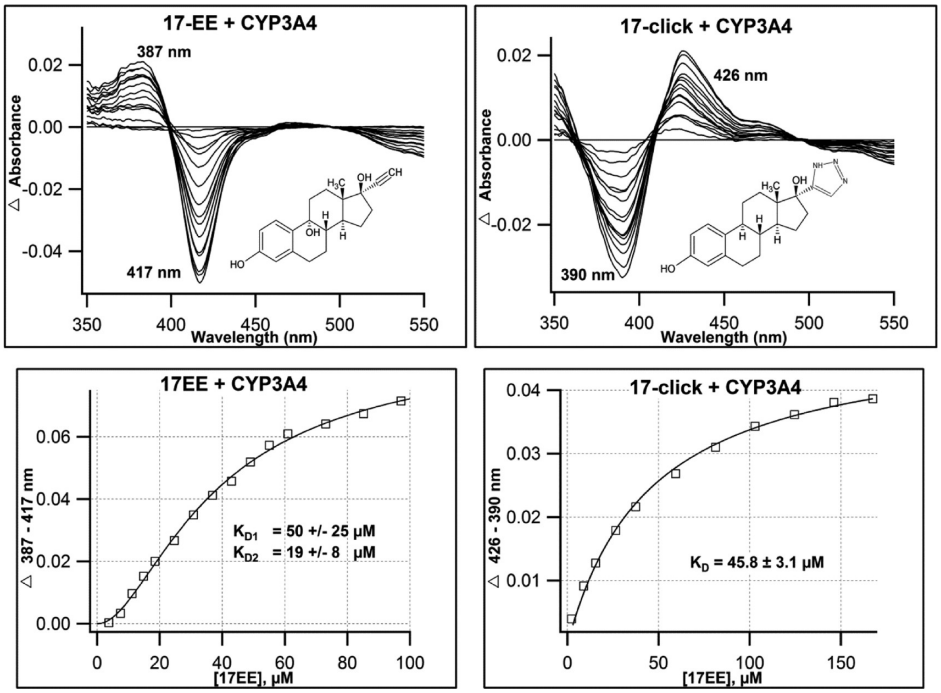

Figure 4. Optical titrations and binding isotherms for binding of 17EE and 17-click to CYP3A4. Installment of the 1,2,3-TRZ fragment on the 17EE framework to yield 17-click induces a type I (17EE, top left) to type II (17-click, top right) equilibrium binding conversion. Titrations were conducted in the presence of 2 μM CYP3A4 (100 mM KP_i and 20% glycerol, pH 7.4, 20 °C): with 17EE (left) and with 17-click (right). The calculated binding isotherm for 17EE (bottom left) fit best to a sequential two-site binding model in which the binding of the first 17EE equivalent is "spin-silent", while the second "spin-audible" equivalent binds with positive cooperativity. The 17-click binding isotherm (bottom right) displays hyperbolic binding behavior with an affinity similar to that of parent 17EE.

Table 3. Comparison of Normalized (1 μM) UV−vis Spectral Data for Binding of 1,2,3-TRZ and 17-Click to CYP3A4

ligand	relative ΔAbs_{390}[a] (1 μM)	Soret red shift (nm)	ΔAbs_{max} (1 μM)[b]
1,2,3-TRZ	1.00	6	0.058
17-click	0.34	2	0.020

[a]Relative intensity change at 390 nm used to approximate the relative efficiency of 1,2,3-TRZ ligands to decrease the inherent high-spin 3A4 fraction (type IIa).[23,24] [b]Peak minus trough intensity from the calculated difference spectrum.

the 1,2,3-TRZ−CYP3A4 complex might correspond to two possible heme ligation states of 1,2,3-TRZ involving either N1(3) or N2, each producing distinct EPR spectra. Interestingly, 17-click produced rather small shifts in EPR g values from those of the ligand-free protein: 2.415 (g_z), 2.249 (g_y), and 1.922 (g_x), with g_z being shifted to a smaller value than the ligand-free enzyme. The results suggest that 1,2,3-TRZ and 17-click, both of which form low-spin CYP3A4 complexes based on optical spectra, do so with distinctly different interactions with the heme iron.

Hyperfine sublevel correlation spectroscopy (HYSCORE) was used to probe further the environment of heme Fe(III) with different ligands using the hyperfine interaction between the unpaired spin on heme iron and nearby nuclei. HYSCORE is a two-dimensional EPR method that allows for detection of the effects of neighboring nuclei on EPR electronic transitions. Specifically, we investigated the protons of the axial H_2O coordinated to the heme that were assigned in previous studies of ligand-free CYP2C9 and CYP101A1 (P450cam).[44,45] Figure 6 shows the HYSCORE spectra of CYP3A4 with no ligand at

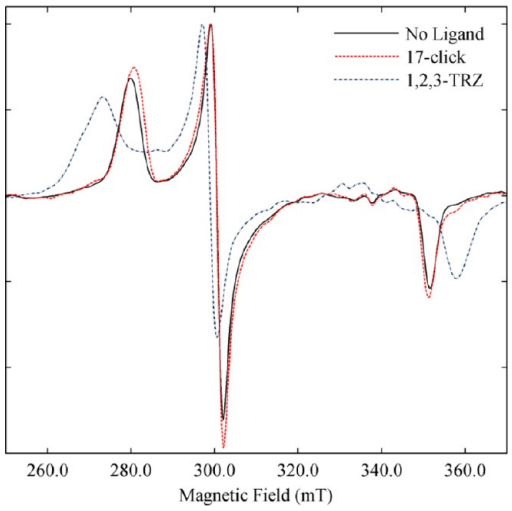

Figure 5. X-Band CW EPR spectra of ligand-free and ligand-bound low-spin CYP3A4. Spectra of ligand-free (black), 1,2,3-TRZ-saturated (blue), and 17-click-saturated (red) forms. For all spectra, the protein concentration was 45 μM in 0.2 M KP_i (pH 7.4, 20% glycerol). All experiments were conducted at 15 K, and the EPR intensities were normalized.

the magnetic field corresponding to g_z for the water-ligated resting enzyme complex. The peaks and arcs extending between frequencies [(9.3, 16.0) and (10.7, 14.5)] and [(16.0, 9.5) and (14.5, 10.9)] MHz indicated by an ellipse have isotropic hyperfine splitting values of 4.31 MHz, estimated from the spectral simulation, that are similar to values reported for protons of the axial water in Fe(III) CYP2C9 and CYP101.[44,45] Detailed analysis of the spectral line shapes[33,34] shows that

dx.doi.org/10.1021/bi300744z | Biochemistry 2012, 51, 6441−6457

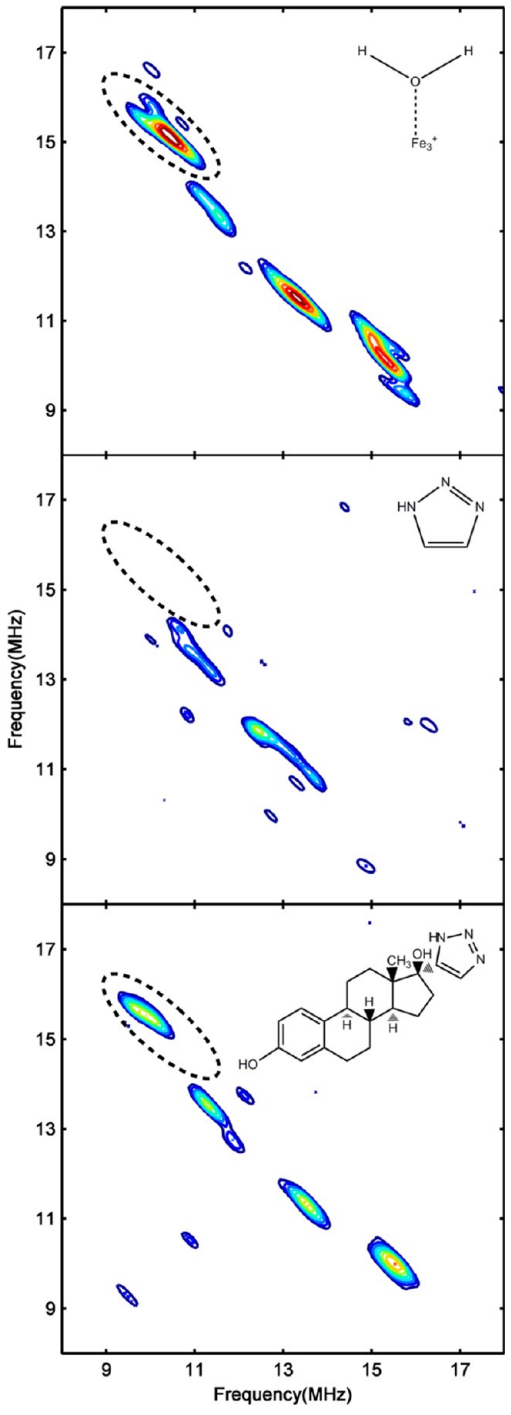

Figure 6. HYSCORE spectra of ligand-free and ligand-bound low-spin CYP3A4 corresponding to g_z. Shown is the proton frequency region of the HYSCORE spectra from ligand-free CYP3A4 (top), CYP3A4 with 50 mM 1,2,3-TRZ (middle), and CYP3A4 with 225 μM 17-click (bottom). Proton signals corresponding to the axial H_2O protons in ligand-free CYP3A4 (top) are defined by an ellipse and are displaced by the type II binding 1,2,3-TRZ fragment (middle). Despite type II binding observed optically, HYSCORE reveals that 17-click binding (bottom) does not displace H_2O from the heme but instead alters its ligand field strength. The protein concentration was 45 μM for all samples. Magnetic field strength: 288.0 mT for the ligand-free form, 283.0 mT with 1,2,3-TRZ, and 287.0 mT with 17-click. All the spectra were normalized to the peaks of highest intensity [i.e., the N2 peak in the (−,+) quadrant].

these signals arise from protons that are 2.65 Å from the heme Fe(III). The remaining signals arise from other protons near the heme. A second set of peaks and arcs extending between frequencies [(10.5, 14.0) and (12.2, 12.5)] and [(12.8, 11.8) and (14.0, 10.8)] MHz has an isotropic hyperfine splitting value of −3.82 MHz and lies 3.05 Å from the heme Fe(III). These signals are tentatively assigned to the thiolate β-protons [Fe(III)-S-CH_2-R] of the cysteine residue axially bound to the heme Fe(III). As a positive type II binding control, the HYSCORE spectrum for the CYP3A4−1,2,3-TRZ complex was obtained, and the proton frequency region of the HYSCORE spectrum at magnetic field strength corresponding to g_z for this complex is also depicted in Figure 6. The HYSCORE spectrum clearly demonstrates displacement of the axial sixth water molecule by the 1,2,3-TRZ fragment by the disappearance of the previously characterized proton peaks and arcs. Unexpectedly, the HYSCORE spectra of CYP3A4 with a saturating concentration of 17-click retain the axial H_2O proton peaks and arcs, with only slight frequency shifts [(9.3, 16.0) and (10.5, 15.0)] and [(15.0, 10.3) and (16.0, 9.5)]. In addition, no new nitrogen interactions were detected by comparison with the ligand-free control spectra. The isotropic hyperfine coupling value obtained from spectral simulation of the shifted proton arcs is −4.02 MHz, which corresponds to axially bound water protons 2.75 Å from heme Fe(III), a slight increase from the distance in the ligand-free state.

These experimental results present a paradox. On one hand, 17-click induces a type II optical spectrum suggestive of direct interaction with the heme iron and displacement of the axial water, yet HYSCORE shows that the protons of the axial water (and the cysteine) are retained when 17-click binds, with small but readily detectable perturbation of both the protons and the EPR g values. 17-Click causes changes in electronic interactions of the heme while the axial water and cysteine remain. It is likely that the field strength of the axial water ligand is altered by hydrogen bonding interactions with the 1,2,3-TRZ moiety of 17-click, which is supported by the lengthening of the OH_2···Fe(III) distance in the 17-click-bound HYSCORE spectra. Possible structural interpretations of this are suggested in Discussion.

17-Click Functional Inhibition of CYP3A4 and Metabolic Stability. 17-Click inhibited CYP3A4-mediated 6β-hydroxylation of testosterone in Supersomes with an IC_{50} of 17 ± 6 μM as determined by the LC−MS/MS assay (Figure S1 of the Supporting Information). To assess metabolic stability, substrate depletion of 2.5 μM 17-click was also monitored and demonstrated facile turnover of the type II ligand with only ∼50% of the compound remaining after a 25 min incubation in the presence of 100 nM CYP3A4 in Supersomes (data not shown). A representative ion current chromatogram for m/z 340 + 16 (O) = 356 from LC−MS/MS analysis of a larger scale incubation is shown in Figure 7 and clearly shows formation of at least four NADPH-dependent metabolites.

To assess the rate of CYP3A4-mediated 17-click turnover, K_M and k_{cat} for total 17-click metabolism were measured by LC−MS/MS using the methods of substrate depletion[18] and found to be 2.5 ± 0.4 μM and 2.1 ± 0.3 min^{-1}, respectively (Figure S2 of the Supporting Information). Our attempts to quantify kinetic parameters for 17EE using the substrate depletion approach were unsuccessful; however, it was observed that depletion rates were between 3- and 10-fold faster for 17EE relative to 17-click at low substrate concentrations, and that significant depletion was still evident

dx.doi.org/10.1021/bi300744z | Biochemistry 2012, 51, 6441−6457

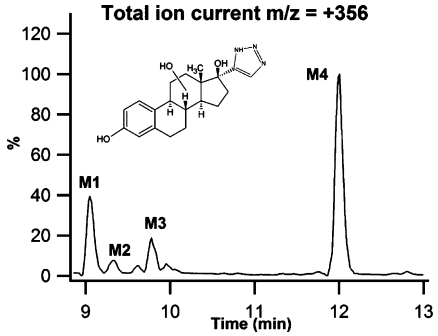

Figure 7. 17-Click metabolites detected during LC−MS/MS analysis [m/z 340 + 16 (O) = 356] of incubations of 17-click in CYP3A4 Supersomes.

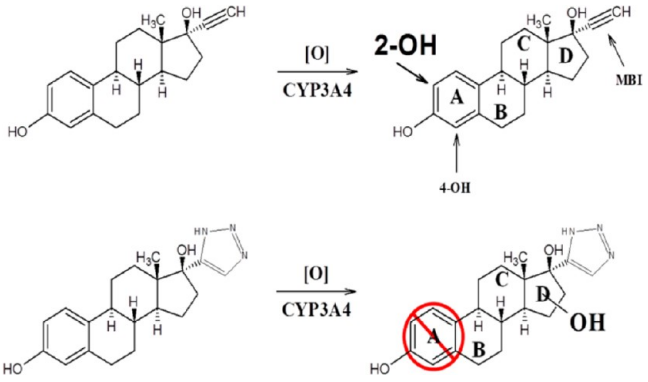

Figure 8. Schematic showing primary sites of oxidative metabolism for parent 17EE and the effect of the addition of the 1,2,3-TRZ fragment on regioselectivity. When the triazole is added, no metabolism occurs on the A-ring but metabolism is directed toward the triazole. Note that the Markush bonded hydroxyl group represents several possible sites of oxidation on or in the vicinity of the steroid D-ring as determined by mass spectrometry (see Results).

for 17EE at high concentrations that render depletion of 17-click negligible (Figure S3 of the Supporting Information). Wang et al. have reported a K_M of 2.5 ± 1.1 μM and a k_{cat} of 0.052 ± 0.007 min^{-1} for CYP3A4-mediated formation of 2-OH 17EE in Supersomes under conditions determined to be linear with respect to both assay time and enzyme concentration.[46] In that study, it was stated that 2-OH 17EE represents more than 90% of the total metabolism under the conditions employed. Our results suggest that induction of type II binding by the addition of a 1,2,3-TRZ fragment to 17EE has most likely slowed metabolism relative to that of the parent molecule by 3−10-fold, but that 17-click remains highly susceptible to oxidative turnover by CYP3A4.

Metabolic Tailoring: Influence of 1,2,3-TRZ on the Oxidative Regioselectivity in CYP3A4. Qualitatively, the number and relative abundance of CYP3A4-mediated 17-click metabolites are similar to that reported by both Lin et al.[47] and Geungerich[48] for 17EE. To compare the regioselectivity of 17EE oxidation with 17-click oxidation, authentic 2-OH and 4-OH 17-click metabolite standards (primary oxidation products for CYP3A4-mediated 17EE turnover[46,47,49]) were synthesized and isolated in 15% (2-OH) and 3% (4-OH) overall yield using procedures adapted from the literature (Materials and Methods).[14,15] The retention times for the 2-OH and 4-OH 17-click standards did not match that for any of the metabolites during LC−qTOF MS anlaysis (data not shown). Thus, metabolism at the preferred 2 and 4 positions of the 17EE steroid A-ring (Figure 8) is abolished by addition of 1,2,3-TRZ to the drug's scaffold. Representative mass spectra obtained from MS^E analysis (Materials and Methods) of the ion at m/z 356.1974 for the 2-OH standard [similar to the 4-OH 17-click spectrum (data not shown)] and predominant oxidized metabolite, M4, observed in the Supersome incubation extract are shown in Figure 9. Also shown for comparison in Figure 9 is the MS^E spectrum for the remaining 17-click parent from the incubation, corresponding to the ion at m/z 340.2025. Table 4 lists the elemental compositions determined from the observed mass of important fragments from each spectrum (vide infra). The spectra for M1, M2, and M3 were similar (Figure S4 of the Supporting Information) to that shown for the most abundant metabolite, M4, with the exception of a prominent fragment ion unique to M4 at m/z 213.1277, consistent with the molecular formula $C_{15}H_{17}O$ (calculated m/z 213.1279, −0.94 ppm).

The MS fragment data allow some additional conclusions to be drawn regarding the structure of the 17-click metabolites. First, while all species investigated (including 17-click) were observed to dehydrate readily [ion at m/z 356 (340) − 18 = 338 (322)], a second facile dehydration step was observed only for the metabolites (Figure S4 of the Supporting Information for spectra of M1−M3) and indicated by a prominent ion at m/z 320 (20−100 relative abundance), which is completely absent from the MS^E spectrum of both 2-OH (Figure 9) and 4-OH (data not shown) 17-click. Fragmentation of the metabolites favors two facile water losses and loss of N_2 (m/z 292), in stark contrast to fragmentation of 2-OH and 4-OH 17-click (and 17-click) that undergo a single dehydration and loss of N_2 [m/z 310 (M1−M4), m/z 294 (17-click)], a species nearly absent from all metabolite fragment ion spectra. In addition, there are spectral shifts from m/z 157.0657 ($C_{11}H_9O$, +2.5 ppm) and m/z 159.0809 ($C_{11}H_{11}O$, −0.6 ppm) present in spectra of 17-click to m/z 173.0602 ($C_{11}H_9O_2$, −0.6 ppm) and m/z 175.0759 ($C_{11}H_{11}O_2$, 0 ppm) observed in spectrum of 2-OH (and 4-OH) 17-click. These observations suggest that hydroxyl groups are retained at estrogen A-ring positions during fragmentation under the experimental conditions used here. Thus, we conclude that CYP3A4-mediated oxidation of 17-click does not occur at the remaining A-ring position to form 1-OH 17-click, a species of which we had no standard for comparison. Further supporting this conclusion is the fact that the spectra for the metabolites are very similar [except for the ion at m/z 213 in M4 spectra (vide infra)] and if the 1-OH 17-click species were for some reason susceptible to facile A-ring dehydration during fragmentation (mass spectrum lacking prominent ions at m/z 173.175 and 310) it would be anticipated to display a distinct fragment ion spectrum due to disruption of aromaticity. Plausible structures determined with MassFragment (see Materials and Methods) for signature fragments that contain the steroid A-ring are shown in the spectra of Figure 9.

Additional structural insight into the identity of the primary metabolite, M4, was made possible via MS^n analysis using an LTQ ion trap instrument. On the basis of two unique ion trapping sequences (m/z 356 → 338 → 320 → fragments and m/z 356 → 338 → 213 → fragments), we concluded that the ion at m/z 213 is a kinetic product formed during fragmentation of the ion at m/z 338, the formation of this species being entirely dependent on the loss of a second equivalent of water from M4 (Scheme 1). The overwhelming relative abundance of the ion at m/z 213 in the fragment ion spectrum of M4, coupled with the complete absence of this (or

dx.doi.org/10.1021/bi300744z | Biochemistry 2012, 51, 6441−6457

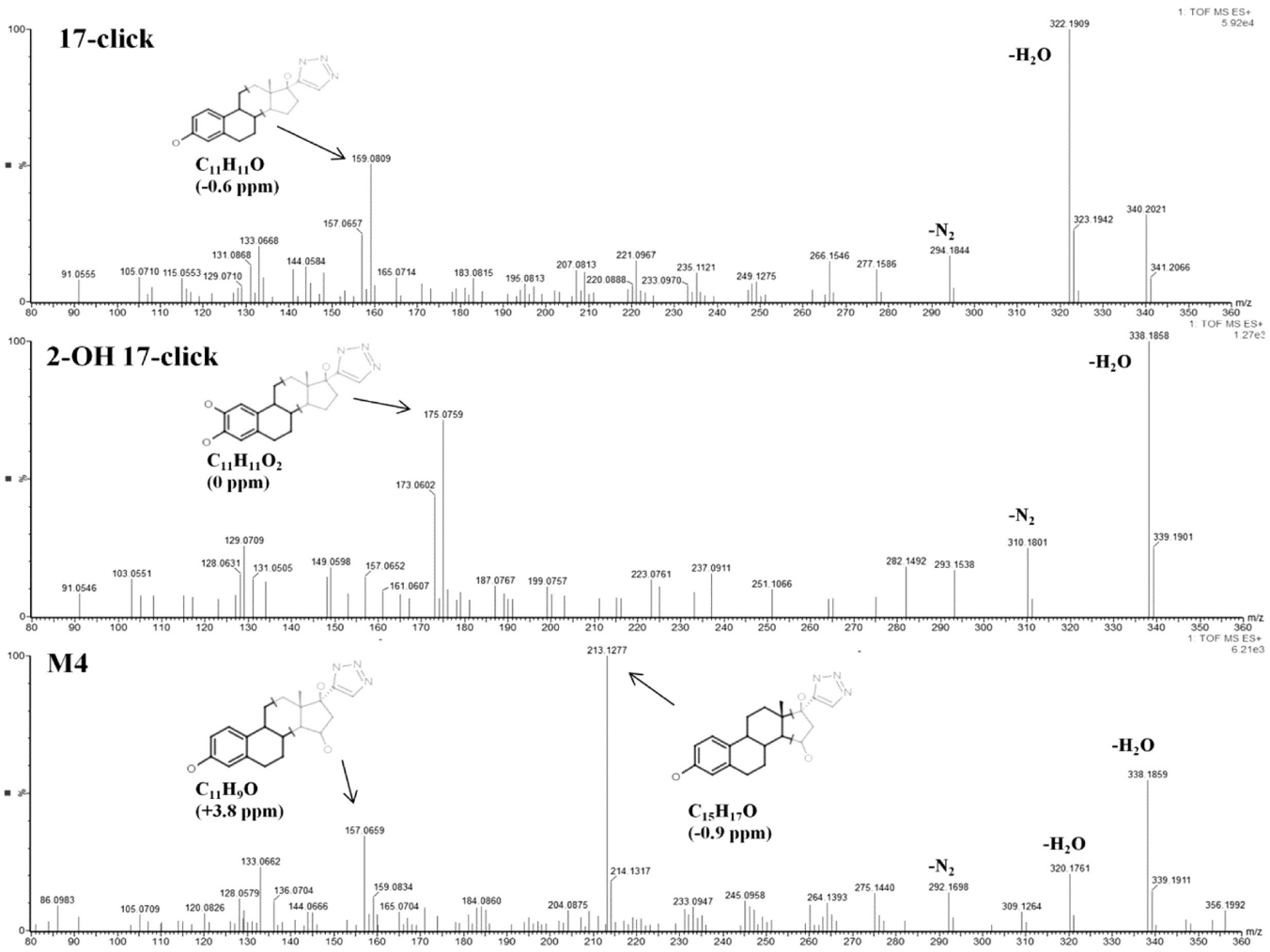

Figure 9. MS^E fragment ion spectra. 17-Click [m/z 340.2025 ($C_{20}H_{26}N_3O_2$)] (top), 2-OH 17-click (middle), and metabolite M4 [m/z 356.1974 ($C_{20}H_{26}N_3O_3$)] (bottom). M4 represents the most abundant metabolite species and that closest in retention time to synthesized 2-OH and 4-OH 17-click. High-resolution mass spectra were acquired using a SYNAPT qTOF mass spectrometer in MS^E mode with a collision energy ramp of 15−45 V (Materials and Methods). Structural proposals for highlighted fragments were obtained using MassFragment in MassLynx. Note that the illustrated D-ring location of CYP3A4-mediated oxidation for M4 is indefinite and merely represents one of a few probable turnover positions near or on the steroid D-ring based on results from ion trapping (vide infra).

Table 4. Elemental Compositions of Key Ions Determined by qTOF MSE Anlaysis of 17-Click, 2-OH 17-Click, and Predominant Metabolite M1

	formula	relative abundance (%)	theoretical	actual	σ (ppm)
17-click	$C_{11}H_9O$	30	157.0653	157.0657	2.5
	$C_{11}H_{11}O$	50	159.0810	159.0809	−0.6
	$C_{20}H_{24}NO$	20	294.1858	294.1844	−4.8
	$C_{20}H_{24}N_3O$	100	322.1919	322.1909	−3.1
	$C_{20}H_{26}N_3O_2$	30	340.2025	340.2021	−1.2
2-OH 17-click	$C_{11}H_9O_2$	30	173.0603	173.0602	−0.6
	$C_{11}H_{11}O_2$	75	175.0759	175.0759	0.0
	$C_{20}H_{24}NO_2$	25	310.1807	310.1801	−1.9
	$C_{20}H_{24}N_3O_2$	100	338.1869	338.1858	−3.3
	$C_{20}H_{26}N_3O_3$	5	356.1974	356.1963	−3.1
M4	$C_{11}H_9O$	40	157.0653	157.0659	3.8
	$C_{15}H_{17}O$	100	213.1279	213.1277	−0.9
	$C_{20}H_{22}NO$	10	292.1701	292.1698	−1.0
	$C_{20}H_{22}N_3O$	15	320.1763	320.1761	−0.6
	$C_{20}H_{24}N_3O_2$	60	338.1869	338.1859	−3.0
	$C_{20}H_{26}N_3O_3$	10	356.1974	356.1971	−0.8

dx.doi.org/10.1021/bi300744z | *Biochemistry* 2012, 51, 6441−6457

Scheme 1. MS^4 Analysis of the Primary CYP3A4-Mediated Metabolite of 17-Click (M4) Reveals a Predominant M1 Daughter Ion (m/z 213) To Be a Kinetic Product of the Second Dehydration Step[a]

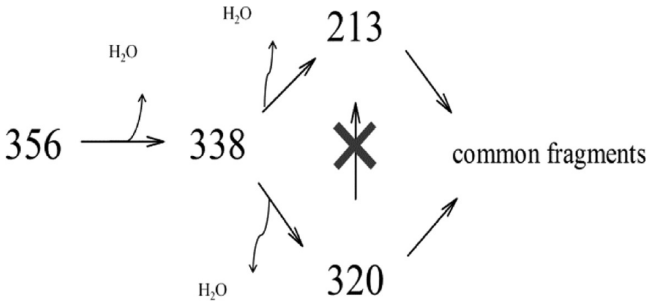

[a]The ion at m/z 213 was entirely absent from MS^4 spectra using the sequence m/z 356 → 338 → 320 → fragment, while the ion remained in 80% relative abundance (data not shown) using the sequence m/z 356 → 338 → 213 → fragment.

equivalent) species in fragment spectra of 17-click, suggests that the required dehydration step to form the ion at m/z 213 involves the oxygen incorporated into the molecule during CYP3A4-mediated turnover. Thus, the structural identity of this fragment should offer insight into the location of oxidative turnover of 17-click. To this end, MassFragment was used to generate a structural proposal (Figure 9) for fragment ion $C_{15}H_{17}O$ (calculated m/z 213.1279, −0.94 ppm), and a structure characterized by fragmentation of the estrogen D-ring of 17-click was determined to be the only plausible solution given the elemental composition of this fragment (see Discussion). In conclusion, addition of a 1,2,3-TRZ−heme interaction in the CYP3A4−17EE complex has eliminated the preferred sites of estrogen metabolism entirely (A-ring) and steered the metabolism predominantly toward the D-ring bearing the triazole moiety.

DISCUSSION

1,2,3-TRZ has received great attention in the drug-design arena[8,9] since the discovery in 2001 of novel catalysts for the well-known 1,3-dipolar cyclo-addition reaction between organic azides and alkynes, or the click reaction. The synthetic advantages to the medicinal chemist, via the methods of click chemistry, have prompted widespread use of 1,2,3-TRZ as a central scaffold moiety in fragment-based drug design for a wide range of targets.[8,50] Interestingly, despite the prevalence in CYP-targeted drugs of the closely related azole congeners IMZ and 1,2,4-TRZ, the efficacy of 1,2,3-TRZ as a CYP pharmacophore has not been established. However, high-affinity interactions of 1,2,3-TRZ with transition metals are known; in fact, 1,2,3-TRZ forms complexes with a variety of transition metals, including both ferrous and ferric iron species.[11] Thus, the first goal of this study was to employ a fragment-based systematic investigation of the relative heme binding affinity, CYP binding thermodynamics, and spectral behavior of 1,2,3-TRZ in comparison to those of established azole CYP pharmacophores IMZ and 1,2,4-TRZ.

Our DFT results suggest that 1,2,3-TRZ interacts less favorably than the other azoles but is competent for type II binding inasmuch as it can be a stronger ligand than water. The in silico energies for the complexes trend with the aqueous basicity of the fragments [IMZ (pK_a = 6.99) > 1,2,4-TRZ (pK_a = 2.45) > 1,2,3-TRZ (pK_a = 1.15)][37]; it was not entirely obvious that this trend should exist because very high basicity (nucleophilicy) for a distal heme ligand might disfavor heme coordination because of the donation of charge from the proximal thiolate.[51] 1,2,3-TRZ−heme complexes were also calculated to have the longest Fe(III)-N bonds, as well as the lowest bond order compared with those of the other fragments (IMZ and 1,2,4-TRZ). One interesting conclusion from the computational studies is that 1,2,3-TRZ is predicted to ligate heme iron at both N1 and N2, suggesting the possibility that two different routes for heme coordination could be active when binding CYP. Recently, an unusually high-affinity (0.018 μM, ligand efficiency of 0.88) 1,2,3-TRZ fragment species, 4-(3-methylphenyl)-1*H*-1,2,3-triazole, was discovered to coordinate two Co^{2+} ions simultaneously in human methionine amino peptidase 2 via N1 and N2 during a fragment-based drug screen.[10] Thus, our DFT results and published work suggest that 1,2,3-TRZ could ligate the heme iron of CYPs in two different modes, with the possibility of substituent effects "steering" ligation to either N1 or N2.

Experimental measures of CYP binding affinity and UV−vis absorbance spectral behavior for 1,2,3-TRZ provided further insight for this azole fragment. In buffered aqueous solution, 1,2,3-TRZ bound with modest affinity (up to 367-fold lower compared with that of 1,2,4-TRZ binding CYP3A4) relative to the other azoles when screened against CYP3A4 and CYP2C9. Spectrally, 1,2,3-TRZ displayed smaller red shifts in both the Soret and α/β band regions, as well as decreased effects on the α:β ratio. The relative spectral behavior of 1,2,3-TRZ−CYP complexes appears to correlate with the lower CYP binding affinity for 1,2,3-TRZ and is likely related to the inferior heme binding energetics observed in our calculations. Interestingly, this comparison highlights a perplexing aspect of the mechanism for binding of small hydrophilic azole fragments to CYPs. Additional equilibrium binding complexity was observed in the isotherms of binding of 1,2,4-TRZ to both CYP2C9 and CYP3A4, corroborating a previous type II binding study by Locuson et al.[23] In that study, the authors speculated that the multiple binding phases observed during equilibrium titration might be explained by considering the multiple nitrogen ligation states that exist for 1,2,4-TRZ. However, similar binding complexity (and similar binding affinity) observed by the authors for the N1-methyl fragment derivative would suggest otherwise; the modification should sterically limit heme ligation to N4 only. The authors also proposed that 1,2,4-TRZ−CYP complexes may exist as a mixture of directly ligated and axial water-bridged complexes at equilibrium, which are anticipated to perturb the heme differentially as was shown in this study for a ligand bearing 1,2,3-TRZ. However, these hypotheses to explain complex equilibrium binding behavior would require a heterogeneous, slowly equilibrating protein population, so multiple bindings of the 1,2,4-TRZ fragment is the more likely explanation. Also described in the study by Locuson et al. was binding isotherm complexity for binding of IMZ to CYP2C9 (WT) at pH 7.4 that could be linearized via adjustment of the pH significantly above the fragment pK_a (6.99[30]). This behavior is not observed for binding of IMZ to the hepta mutant CYP2C9 used here. This discrepancy may reflect modest differences in active site structure for the wild type versus the mutant proteins. Also puzzling is the fact that the rank order CYP3A4 affinity measured here for IMZ and 1,2,4-TRZ was reversed relative to that from the DFT calculations, with the first equivalent (two-site sequential model) of 1,2,4-TRZ binding with greater

affinity than IMZ. These results, together with the thermodynamic studies, highlight the important contributions of protein architecture to fragment−CYP binding energetics.

The chemical similarity between IMZ and 1,2,3-TRZ allows for a meaningful comparison of enthalpic ($\Delta H°$) and entropic ($\Delta S°$) components of their binding affinities. Therefore, van 't Hoff analysis was employed to obtain thermodynamic signatures for the CYP3A4 binding interaction. We observed a linear temperature dependence of equilibrium binding constants for these small hydrophilic azole fragments, suggesting that heat capacity changes ($\Delta C_p°$) for fragment-bound complexes are negligible, at least over the temperature range studied here. A negligible heat capacity change (constant $\Delta H°$ and $\Delta S°$) upon formation of azole fragment−CYP3A4 complexes is consistent with the hydrophilic nature of IMZ and 1,2,3-TRZ, as well as their small size that is not expected to induce conformational changes when ligated to heme iron.[43] Our thermodynamic results are informative on several levels. First, we found that the large discrepancy in $\Delta G°$ between binding of IMZ and 1,2,3-TRZ (−5.1 vs −2.3 kcal/mol at 25 °C) to CYP3A4 in 100 mM KP_i is dictated by a much larger entropic penalty for binding in the case of 1,2,3-TRZ; surprisingly, the ΔH term is slightly more favorable for 1,2,3-TRZ binding than IMZ, but the entropic difference makes a major contribution to their differential affinities. It is tempting to speculate that this phenomenon could be related to the well-documented 1,2,3-TRZ tautomeric complexity. 1,2,3-TRZ tautomerism is known to be highly dependent on solvent type, polarity, temperature, and 1,2,3-TRZ concentration.[40,41,52,53] In dilute aqueous environments, 1,2,3-TRZ exists at an ∼1:1 ratio of degenerate N1(3)-H tautomers, and the N2-H tautomer.[41] Binding of the 1,2,3-TRZ fragment to protein may disrupt this equilibrium mixture toward the selection of a single tautomeric form, presumably the symmetric N2-H tautomer that predominates in low-dielectric solvents. Additionally, if ligation to heme iron is favored at the more basic nitrogen positions (N1 and N3), then a tautomeric shift opposite to that induced by fragment binding can be expected. A large unfavorable $\Delta S°$ value of −16.5 cal mol^{-1} K^{-1} has been reported for the tautomerization toward the asymmetric N1(N3)-H tautomer in toluene.[40] Next, the magnitudes of $\Delta H°$ and $\Delta S°$ measured for the binding of 1,2,3-TRZ and IMZ fragments to CYP3A4 in KP_i are comparable to those values reported in a previous solution thermodynamic study of small, IMZ-based ligands for CYP2B4.[54] Notably, in that study, the enthalpic signatures (25 °C) of phenylimidazole (PI) species 1-PI and 4-PI were either minimally effected (1-CPI, $\Delta\Delta H°_{binding}$ = −0.07 kcal/mol) or dramatically attenuated (4-CPI, $\Delta\Delta H°_{binding}$ = 2.12 kcal/mol) by chloro substitution, suggesting that addition of relatively lipophilic peripheral substituents contributes mostly toward increased, favorable, $\Delta S°_{binding}$, often at the expense of $\Delta H°_{binding}$, a parameter that, in the case of small, rigid, type II ligands such as 1,2,3-TRZ and IMZ, may be expected to be dominated by coordinate bond formation. An additional source of the larger entropic penalty for 1,2,3-TRZ may be the remaining localized water molecule observed by HYSCORE. These results have particular importance in the context of fragment-based drug design strategies that incorporate click chemistry, for CYP inhibitors as well as other targets. The observation that the difference in binding free energy between IMZ and 1,2,3-TRZ is largely entropic provides an obvious strategy for incrementally improving the affinity of 1,2,3-TRZs; incorporation of hydrophobic groups would likely decrease the entropic cost of binding and increase their affinity very substantially as observed with CYP2B4 and phenylimidazoles.

To test whether 1,2,3-TRZ−heme binding interactions are sufficient to dictate overall ligand positioning of druglike molecules, we sought an ideal molecular framework for 1,2,3-TRZ derivatization to use as a model. 17α-Ethynylestradiol (17EE) was selected for derivatization because of its well-described metabolic profile that allows for some assumptions concerning the molecular details of binding to be inferred. First, 17EE binds in multiple orientations, based on the reported oxidation profile that includes oxygenation on both the estrogen A-ring (2-OH predominant)[46,48,49] and the acetylenic function of the steroid D-ring,[47] which imparts its behavior as a mechanism-based inactivator. However, the combination of the ligand's relatively modest partition ratio of ∼50, low off-target protein adduction, the lack of reported acetylene-derived carboxylic acid metabolites,[47] and overwhelming production of 2-OH 17EE[46−48] all suggest that the estrogen prefers to bind with its A-ring nearest heme.

The UV−vis binding results for 17-click are striking. On the basis of the historical precedent with nitrogen heterocycles, the type II spectrum induced suggests that the D-ring portion of the molecule now lies nearest the heme to yield an additional coordinate bonding interaction that is not possible in 17EE. In the context of a single heme binding site, this would suggest that the addition of the 1,2,3-TRZ causes the estradiol to adopt a different orientation with the TRZ moiety near the heme iron. However, our results are complicated by multiple bindings for 17EE, yet binding of the first equivalent of 17EE induces a negligible heme spin shift, suggesting our comparison is localized at the catalytically relevant site. Regardless of this complexity, it is completely clear that throughout the binding isotherm the high-spin state is favored. Regardless of the correct binding model, it is interesting that, despite the dramatic reversal of the UV−vis binding spectrum to type II for 17-click, no significant increase in ligand affinity was observed. Thus, the TRZ group does not significantly add binding affinity but rather changes the binding mode of the steroid nucleus in a nearly isoenergetic complex. An additional observation of some importance is that the 17-click low-spin complex yields a low-spin difference spectrum with an intensity lower than that of the 1,2,3-TRZ fragment. We considered the possibility that this could be due to "incomplete" heme coordination, as suggested by others.[23] The difference spectra for 17EE are less red-shifted and less intense than the spectra obtained from the fragment (Table 3).

CW and pulsed EPR techniques proved to be invaluable for understanding the binding and turnover behavior of the 17-click−CYP3A4 complex. The CW EPR spectra show that 1,2,3-TRZ and 17-click induce entirely different perturbations in the EPR g values, suggesting that 1,2,3-TRZ−heme interactions are not conserved when present on a drug scaffold. Most profound were the results of HYSCORE analysis that showed conclusively that the 17-click low-spin complex perturbs, yet retains, its axial water ligand. The perturbations of the axial water ligand proton hyperfine splitting values reveal a significant increase in the Fe(III)−H distance of 0.1 Å (from 2.65 to 2.75 Å), consistent with hydrogen bonding between the 1,2,3-TRZ fragment of 17-click and axial water. Thus, the 17-click−CYP3A4 complex is thought to exist at equilibrium as a water-bridged type II ternary complex in which the heme field is perturbed indirectly toward the low-spin state via alteration

dx.doi.org/10.1021/bi300744z | Biochemistry 2012, 51, 6441−6457

of the axial water ligand field strength. This implies that the type II optical spectrum observed is the result of the axial water ligand with increased basicity (stronger field ligand) in the presence of 17-click. A similar water-ligated type II complex was observed by Seward et al. between 1,2,4-TRZ antifungal drug fluconazole[55] and CYP121 of *Mycobacterium tuberculosis*. In that study, a mixture of water-bridged and directly ligated ligand-bound forms was observed in the crystal structure at 1.90 Å resolution. Notably, our EPR and HYSCORE results reveal a homogeneous low-spin protein fraction, suggesting a preferred ligation state for 17-click. It is intriguing to speculate that this phenomenon might be more common than previously believed based on the type II spectrum obtained by UV−vis absorbance, which is not distinguishable from many type II spectra in the literature. Additionally, a review of the earlier P450cam literature reveals similar EPR behavior reported for binding of sterically hindered nitrogen heterocycles, at the time classified as "abnormal" type II ligands.[56] The CW EPR and HYSCORE results are thus entirely consistent with a lack of an increase in affinity upon derivatization of 17EE.

The metabolism of 17-click was studied to determine the functional consequences of this unusual heme ligation. In contrast to our expectation that 17-click would dramatically inhibit CYP activity, the estimated turnover number (k_{cat}) of 2.5 min^{-1} for total metabolism demonstrates that 17-click is a good substrate from CYP3A4. In fact, comparison of depletion data obtained for CYP3A4-mediated 17EE oxidation suggests that the rate of 17-click turnover is only moderately slower for the low-spin ligand. This result is similar to recent work by Jones et al., who found nitrogen-ligated, type II spectral complexes are rapidly metabolized.[5] Because the spectral results demonstrate that the 1,2,3-TRZ moiety of 17-click interacts with heme via H_2O, we found it surprising that the number and relative abundance of the metabolites initially observed were so similar to those observed by others for 17EE.

A combination of high-mass accuracy qTOF and ion trapping (LTQ) mass spectrometries was used to determine structural features of the metabolites. First, comparison of the fragmentation behavior of 17-click and synthesized 2-OH and 4-OH 17-click standards with that of the observed 17-click metabolites allowed us to conclude that steroid A-ring metabolism had been completely abolished for the 1,2,3-TRZ derivative. Second, through ion trapping it was determined that the predominant ion observed in the fragment ion spectrum of M4 originated via loss of the metabolically inserted oxygen atom, and thus, probable structures for this fragment ion that were generated based on elemental composition of this fragment via high-mass accuracy qTOF measurements were used to infer the regioselectivity of CYP3A4-mediated oxidation of 17-click. A structure resulting from oxidation in the vicinity of the steroid D-ring was determined to be the only plausible solution for the primary metabolite, M4. Therefore, the mass spectral data support the conclusion that installation of 1,2,3-TRZ upon the 17EE scaffold alters ligand positioning.

In summary, the 1,2,3-TRZ fragment that is isosteric with imidazole and 1,2,4-TRZ fragments found in a wide range of drugs, including those intended to inhibit CYPs, is chemically competent to ligate to the heme of CYPs. However, when the 1,2,3-TRZ fragment is incorporated on the scaffold of 17EE, EPR spectra indicate that there is not direct nitrogen ligation. Rather, in the presence of the 1,2,3-TRZ-containing 17-click, the sixth axial water is retained and is likely hydrogen bonded to the triazole. This complex, surprisingly, undergoes rapid metabolism, with a regioselectivity different from that of 17EE. Together, the results indicate the potential for novel heme coordination by 1,2,3-TRZ when installed on a CYP substrate. These results, combined with recent findings published by others,[5,6] suggest that low-spin, "type II" complexes should not be assumed to be inhibitory. Most importantly, we present only the second case, and the first direct EPR-based evidence in the form of HYSCORE, of a triazole ligand that elicits a classic type II UV−vis signature indirectly via heme interactions mediated by the axial H_2O ligand. Further studies are required to determine whether the bridged water−heme ligation structure is a general feature of ligands containing the 1,2,3-TRZ fragment.

■ ASSOCIATED CONTENT

Supporting Information

Plots of IC_{50}, and K_m and V_{max} determination by substrate depletion for 17-click; depletion time courses for 17-click and 17EE; and representative MS/MS spectra for 17-click metabolites M1−M3. This material is available free of charge via the Internet at http://pubs.acs.org.

■ AUTHOR INFORMATION

Corresponding Author

*E-mail: winky@uw.edu. Phone: (206) 685-0379.

Funding

This work was supported by National Institute of General Medical Sciences Grant P0132165 and National Institutes of Health Grant TG07752.

Notes

The authors declare no competing financial interest.

■ ACKNOWLEDGMENTS

We thank Dr. Josh T. Pearson for his generous contribution of experimental materials and use of instrumentation, as well as helpful discussion. We also thank Rob Foti, John Davis, Dr. Brooke VandenBrink, and Dr. Dan Rock for assistance in data aquisition and helpful discussion. Finally, the authors thank Dr. Arthur Roberts for his gift of time and discussion related to software implementation for data analysis, as well as Dr. Abhinav Nath for helpful discussion.

■ ABBREVIATIONS

KP_i, potassium phosphate; 1,2,3-TRZ, 1*H*-1,2,3-triazole; 1,2,4-TRZ, 1*H*-1,2,4-triazole; IMZ, imidazole; HYSCORE, hyperfine sublevel correlation spectroscopy; EPR, electron paramagnetic spectroscopy.

■ REFERENCES

(1) Cole, P. A., and Robinson, C. H. (1990) Mechanism and inhibition of cytochrome P-450 aromatase. *J. Med. Chem. 33*, 2933−2942.

(2) Koltin, Y., and Hitchcock, C. A. (1997) The search for new triazole antifungal agents. *Curr. Opin. Chem. Biol. 1*, 176−182.

(3) Ouellet, H., Johnston, J. B., and Ortiz de Montellano, P. R. (2010) The *Mycobacterium tuberculosis* cytochrome P450 system. *Arch. Biochem. Biophys. 493*, 82−95.

(4) Olkkola, K. T., Ahonen, J., and Neuvonen, P. J. (1996) The effects of the systemic antimycotics, itraconazole and fluconazole, on the pharmacokinetics and pharmacodynamics of intravenous and oral midazolam. *Anesth. Analg. (Hagerstown, MD, U.S.) 82*, 511−516.

(5) Peng, C.-C., Pearson, J. T., Rock, D. A., Joswig-Jones, C. A., and Jones, J. P. (2010) The effects of type II binding on metabolic stability

and binding affinity in cytochrome P450 CYP3A4. *Arch. Biochem. Biophys. 497*, 68−81.
(6) Pearson, J., Dahal, U. P., Rock, D., Peng, C.-C., Schenk, J. O., Joswig-Jones, C., and Jones, J. P. (2011) The kinetic mechanism for cytochrome P450 metabolism of Type II binding compounds: Evidence supporting direct reduction. *Arch. Biochem. Biophys. 511*, 69−79.
(7) Peng, C.-C., Shi, W., Lutz, J. D., Kunze, K. L., Liu, J. O., Nelson, W. L., and Isoherranen, N. (2012) Stereospecific metabolism of itraconazole by CYP3A4: Dioxolane ring scission of azole antifungals. *Drug Metab. Dispos. 40*, 426−435.
(8) Meldal, M., and Tornoe, C. W. (2008) Cu-catalyzed azide alkyne cycloaddition. *Chem. Rev. 108*, 2952−3015.
(9) Kolb, H. C., and Sharpless, K. B. (2003) The growing impact of click chemistry on drug discovery. *Drug Discovery Today 8*, 1128−1137.
(10) Congreve, M., Chessari, G., Tisi, D., and Woodhead, A. J. (2008) Recent developments in fragment-based drug discovery. *J. Med. Chem. 51*, 3661−3680.
(11) Moore, D. S., and Robinson, S. D. (1988) Catenated Nitrogen Ligands Part II: Transition Metal Derivatives of Triazoles, Tetrazoles, Pentazoles, and Hexazine. In *Advances in Inorganic Chemistry* (Sykes, A. G., Ed.) pp 171−239, Academic Press, San Diego.
(12) Woods, C. M., Fernandez, C., Kunze, K. L., and Atkins, W. M. (2011) Allosteric activation of cytochrome P450 3A4 by α-naphthoflavone: Branch point regulation revealed by isotope dilution analysis. *Biochemistry 50*, 10041−10051.
(13) Williams, P. A., Cosme, J., Ward, A., Angove, H. C., Matak Vinkovic, D., and Jhoti, H. (2003) Crystal structure of human cytochrome P450 2C9 with bound warfarin. *Nature 424*, 464−468.
(14) Tienan, J., Shin, K., and Yoshinori, Y. (2004) Copper-catalyzed synthesis of *N*-unsubstituted 1,2,3-triazoles from nonactivated terminal alkynes. *Eur. J. Org. Chem. 2004*, 3789−3791.
(15) Rugang, X., Qiuyun, C., Jin, X., and Huaming, Z. (1990) A new efficient synthetic method for 2- and 4-hydroxy-17α-ethynylestradiol. *Steroids 55*, 488−490.
(16) Noble, R. W., and Gibson, Q. H. (1970) The Reaction of Ferrous Horseradish Peroxidase with Hydrogen Peroxide. *J. Biol. Chem. 245*, 2409−2413.
(17) Obach, R. S., and Reed-Hagen, A. E. (2002) Measurement of Michaelis constants for cytochrome P450-mediated biotransformation reactions using a substrate depletion approach. *Drug Metab. Dispos. 30*, 831−837.
(18) Nath, A., and Atkins, W. M. (2006) A theoretical validation of the ssubstrate depletion approach to determining kinetic parameters. *Drug Metab. Dispos. 34*, 1433−1435.
(19) Zhao, Y., and Truhlar, D. G. (2008) Density Functionals with Broad Applicability in Chemistry. *Acc. Chem. Res. 41*, 157−167.
(20) Swart, M., Guell, M., Luis, J. M., and Sola, M. (2010) Spin-state-corrected Gaussian-type orbital basis sets. *J. Phys. Chem. A 114*, 7191−7197.
(21) Bode, B. M., and Gordon, M. S. (1998) Macmolplt: A graphical user interface for GAMES. *J. Mol. Graphics Modell. 16*, 133−138.
(22) Das, A., Zhao, J., Schatz, G. C., Sligar, S. G., and Van Duyne, R. P. (2009) Screening of type I and II drug binding to human cytochrome P450-3A4 in nanodiscs by localized surface plasmon resonance spectroscopy. *Anal. Chem. 81*, 3754−3759.
(23) Locuson, C. W., Hutzler, J. M., and Tracy, T. S. (2007) Visible spectra of type II cytochrome P450-drug complexes: Evidence that "incomplete" heme coordination is common. *Drug Metab. Dispos. 35*, 614−622.
(24) Schenkman, J. B. (1970) Nature of the type I and II spectral changes in liver microsomes. *Biochemistry 9*, 2081−2091.
(25) Roberts, A. G., Sjögren, S. E. A., Fomina, N., Vu, K. T., Almutairi, A., and Halpert, J. R. (2011) NMR-derived models of amidopyrine and its metabolites in complexes with rabbit cytochrome P450 2B4 reveal a structural mechanism of sequential N-dealkylation. *Biochemistry 50*, 2123−2134.
(26) Roberts, A. G., Yang, J., Halpert, J. R., Nelson, S. D., Thummel, K. T., and Atkins, W. M. (2011) The structural basis for homotropic and heterotropic cooperativity of midazolam metabolism by human cytochrome P450 3A4. *Biochemistry 50*, 10804−10818.
(27) Davydov, D. R., Deprez, E., Hoa, G. H. B., Knyushko, T. V., Kuznetsova, G. P., Koen, Y. M., and Archakov, A. I. (1995) High-pressure-induced transitions in microsomal cytochrome P450 2B4 in solution: Evidence for conformational inhomogeneity in the oligomers. *Arch. Biochem. Biophys. 320*, 330−344.
(28) Fukada, H., and Takahashi, K. (1998) Enthalpy and heat capacity changes for the proton dissociation of various buffer components in 0.1 M potassium chloride. *Proteins: Struct., Funct., Bioinf. 33*, 159−166.
(29) Helgeson, H. C., and Kirkham, D. H. (1974) Theoretical prediction of the thermodynamic behavior of aqueous electrolytes at high pressures and temperatures; II, Debye-Huckel parameters for activity coefficients and relative partial molal properties. *Am. J. Sci. 274*, 1199−1261.
(30) Robert, N. G., Nand, K., and Rebecca, M. L. (2002) Thermodynamic quantities for the ionization reactions of buffers. *J. Phys. Chem. Ref. Data 31*, 231−370.
(31) Clarke, E. C. W., and Glew, D. N. (1966) Evaluation of thermodynamic functions from equilibrium constants. *Trans. Faraday Soc. 62*, 539−547.
(32) Bowman, M. K. (2009) Pulsed Electron Paramagnetic Resonance. In *Electron Paramagnetic Resonance: A Practitioner's Toolkit* (Brustalon, M., and Giamello, E., Eds.) pp 159−194, John Wiley & Sons, Hoboken, NJ.
(33) Dikanov, S. A., and Bowman, M. K. (1995) Cross-peak lineshape of two-dimensional ESEEM spectra in disordered S = 1/2, I = 1/2 spin system. *J. Magn. Reson., Ser. A 116*, 125−128.
(34) Dikanov, S. A., Tyryshkin, A. M., and Bowman, M. K. (2000) Intensity of cross-peaks in HYSCORE spectra of S = 1/2, I = 1/2 spin systems. *J. Magn. Reson. 144*, 228−242.
(35) Stoll, S., and Schweiger, A. (2006) EasySpin, a comprehensive software package for spectral simulation and analysis in EPR. *J. Magn. Reson. 178*, 42−55.
(36) Hariharan, P. C., and Pople, J. A. (1973) The influence of polarization functions on molecular orbital hydrogenation energies. *Theor. Chem. Acc. 28*, 213−222.
(37) Catalan, J., and Elguero, J. (1987) Basicity and acidity of azoles. In *Advances in Heterocyclic Chemistry*, Vol. *41*, pp 187−274, Academic Press, San Diego.
(38) Gillam, E. M. J., Baba, T., Kim, B. R., Ohmori, S., and Guengerich, F. P. (1993) Expression of modified human cytochrome P450 3A4 in *Escherichia coli* and purification and reconstitution of the enzyme. *Arch. Biochem. Biophys. 305*, 123−131.
(39) Peng, C.-C., Cape, J. L., Rushmore, T., Crouch, G. J., and Jones, J. P. (2008) Cytochrome P450 2C9 type II binding studies on quinoline-4-carboxamide analogues. *J. Med. Chem. 51*, 8000−8011.
(40) Lunazzi, L., Parisi, F., and Macciantelli, D. (1984) Conformational studies by dynamic nuclear magnetic resonance spectroscopy. Part 27. Kinetics and mechanism of annular tautomerism in isomeric triazoles. *J. Chem. Soc., Perkin Trans. 2,*, 1025−1028.
(41) Minkin, V. I., Garnovskii, A. D., Elguero, J., Katritzky, A. R., and Denisko, O. V. (2000) The Tautomerism of Heterocycles: Five-Membered Rings with Two or More Heteroatoms. In *Advances in Heterocyclic Chemistry*, Vol. *76*, pp 159−214, Academic Press, San Diego.
(42) Roberts, A. G., Campbell, A. P., and Atkins, W. M. (2005) The thermodynamic landscape of testosterone binding to cytochrome P450 3A4: Ligand binding and spin state. *Biochemistry 44*, 1353−1366.
(43) Williams, P. A., Cosme, J., Vinkovic, D. M., Ward, A., Angove, H. C., Day, P. J., Vonrhein, C., Tickle, I. J., and Jhoti, H. (2004) Crystal structures of human cytochrome P450 3A4 bound to metyrapone and progesterone. *Science 305*, 683−686.
(44) Goldfarb, D., Bernardo, M., Thomann, H., Kroneck, P. M. H., and Ullrich, V. (1996) Study of water binding to low-spin Fe(III) in

cytochrome P450 by pulsed ENDOR and four-pulse ESEEM spectroscopies. *J. Am. Chem. Soc. 118*, 2686−2693.
(45) Roberts, A. G., Cheesman, M. J., Primak, A., Bowman, M. K., Atkins, W. M., and Rettie, A. E. (2010) Intramolecular heme ligation of the cytochrome P450 2C9 R108H mutant demonstrates pronounced conformational flexibility of the B-C loop region: Implications for substrate binding. *Biochemistry 49*, 8700−8708.
(46) Wang, B., Sanchez, R. I., Franklin, R. B., Evans, D. C., and Huskey, S.-E. W. (2004) The Involvment of CYP3A4 and CYP2C9 in the metabolism of 17-ethinylestradiol. *Drug Metab. Dispos. 32*, 1209−1212.
(47) Lin, H.-l., Kent, U. M., and Hollenberg, P. F. (2002) Mechanism-based inactivation of cytochrome P450 3A4 by 17α-ethynylestradiol: Evidence for heme destruction and covalent binding to protein. *J. Pharmacol. Exp. Ther. 301*, 160−167.
(48) Guengerich, F. P. (1988) Oxidation of 17α-ethynylestradiol by human liver cytochrome P-450. *Mol. Pharmacol. 33*, 500−508.
(49) Guengerich, F. P. (1990) Metabolism of 17α-ethynylestradiol in humans. *Life Sci. 47*, 1981−1988.
(50) Krasinski, A., Radic, Z., Manetsch, R., Raushel, J., Taylor, P., Sharpless, K. B., and Kolb, H. C. (2005) In situ selection of lead compounds by Click chemistry: Target-guided optimization of acetylcholinesterase inhibitors. *J. Am. Chem. Soc. 127*, 6686−6692.
(51) Sono, M., and Dawson, J. H. (1982) Formation of low spin complexes of ferric cytochrome P-450-CAM with anionic ligands. Spin state and ligand affinity comparison to myoglobin. *J. Biol. Chem. 257*, 5496−5502.
(52) Tomas, F., Abboud, J. L. M., Laynez, J., Notario, R., Santos, L., Nilsson, S. O., Catalan, J., Claramunt, R. M., and Elguero, J. (1989) Tautomerism and aromaticity in 1,2,3-triazoles: The case of benzotriazole. *J. Am. Chem. Soc. 111*, 7348−7353.
(53) Wofford, D. S., Forkey, D. M., and Russell, J. G. (1982) Nitrogen-15 NMR spectroscopy: Prototropic tautomerism of azoles. *J. Org. Chem. 47*, 5132−5137.
(54) Muralidhara, B. K., Negi, S., Chin, C. C., Braun, W., and Halpert, J. R. (2006) Conformational flexibility of mammalian cytochrome P4502B4 in binding imidazole inhibitors with different ring chemistry and side chains: Solution thermodynamics and molecular modeling. *J. Biol. Chem. 281*, 8051−8061.
(55) Seward, H. E., Roujeinikova, A., McLean, K. J., Munro, A. W., and Leys, D. (2006) Crystal structure of the *Mycobacterium tuberculosis* P450 CYP121-Fluconazole complex reveals new azole drug-P450 binding mode. *J. Biol. Chem. 281*, 39437−39443.
(56) Dawson, J. H., Andersson, L. A., and Sono, M. (1982) Spectroscopic investigations of ferric cytochrome P-450-CAM ligand complexes. Identification of the ligand trans to cysteinate in the native enzyme. *J. Biol. Chem. 257*, 3606−3617.